Key Points:
- A new AI-based method (SAED-ViT) classifies droughts using satellite data without labeled training data sets
- The model identifies major drought years (2011, 2017, 2022) in the Horn of Africa with strong spatial and temporal accuracy
- SAED-ViT correlates strongly with SPEI and outperforms traditional drought indices like NDVI, TCI, and VHI

Correspondence to:
S. Jin,
sgjin@hpu.edu.cn;
sg.jin@yahoo.com

Author Contributions:
Conceptualization: Nasser
A. M. Abdelrahim
Data curation: Nasser A. M. Abdelrahim
Formal analysis: Nasser
A. M. Abdelrahim
Funding acquisition: Shuanggen Jin
Investigation: Shuanggen Jin
Methodology: Nasser A. M. Abdelrahim
Project administration: Shuanggen Jin
Resources: Shuanggen Jin
Software: Nasser A. M. Abdelrahim
Supervision: Shuanggen Jin
Validation: Nasser A. M. Abdelrahim
Visualization: Nasser A. M. Abdelrahim

A Self-Supervised Seasonal Anomaly Embedding ViT for Label-Free Drought Mapping in the Horn of Africa

Nasser A. M. Abdelrahim[1,2,3] ![ORCID], **Shuanggen Jin**[1,4] ![ORCID], **and Shiyu Li**[1,2]

[1]Shanghai Astronomical Observatory, Chinese Academy of Sciences, Shanghai, China, [2]School of Astronomy and Space Science, University of Chinese Academy of Sciences, Beijing, China, [3]Civil Engineering Department, Faculty of Engineering, Sohag University, Sohag Al Gadida, Egypt, [4]School of Surveying and Land Information Engineering, Henan Polytechnic University, Jiaozuo, China

Abstract Drought poses a major threat to agriculture and food security in the Horn of Africa (HOA), where monitoring efforts are hindered by sparse in situ observations and a lack of ground truth data. In this paper, a new self-supervised drought classification model, Seasonal Anomaly Embedding with Vision Transformers (SAED-ViT) is proposed using satellite-derived seasonal anomalies of NDVI, Land Surface Temperature (LST), and precipitation. The method employs the masked autoencoders with Vision Transformers (MAE-ViT) to learn robust spatiotemporal representations from 25 years of satellite Earth observation data (2000–2024). The learned latent features are clustered using unsupervised K-Means to identify semantically meaningful drought regimes, which are then mapped to standardized severity classes without requiring predefined thresholds or labeled data. The results exhibit high spatial accuracy and temporal coherence across a broad range of agro-climatic regions with capturing the large-scale droughts in 2011, 2017, and 2022. Quantitatively compared and verified against Standardized Precipitation Evapotranspiration Index (SPEI), the agreement is strong ($r = -0.91$, P-value < 0.01) and better when compared to the conventional indexes like NDVI, TCI, and VHI. SAED-ViT achieved robust and label-free drought-severity classification across multiple satellite data sources.

Plain Language Summary Droughts are a serious problem in the Horn of Africa, especially because it's hard to monitor them with few ground-based weather stations and limited on-the-ground data. In this study, we introduce a new method called SAED-ViT, which uses satellite data and artificial intelligence to detect and classify droughts without needing labeled training data. Our model incorporates satellite imagery of seasonal vegetation variations (NDVI), surface temperature (LST), and precipitation obtained over the last 25 years (2000–2024). It learns significant patterns in these data by applying the method of masked autoencoders using Vision Transformers and subsequently aggregates the outcomes into various drought classes based on K-Means clustering. These classes correspond to actual drought conditions, although we did not employ classical drought labels. Our approach correctly identified 2011, 2017, and 2022 as severe drought years and highly correlated with the acclaimed SPEI drought index. Actually, it performed better than other traditional drought indices like NDVI, TCI, and VHI. Our approach offers a strong, automatic technique for mapping and tracking droughts in regions where traditional monitoring is not feasible or available.

1. Introduction

Drought is one of the most pressing environmental and socioeconomic challenges facing African countries (Agarwal et al., 2025; Alito & Kerebih, 2024; Jiang et al., 2025). Drought is a multifaceted hazard that extends beyond simple precipitation deficits, encompassing meteorological, agricultural, hydrological, and socio-economic dimensions that collectively disrupt ecosystems, agriculture, and livelihoods (Abdelrahim & Jin, 2025a; Z. Dong & Jin, 2021; Edokossi et al., 2024; Jin et al., 2025; Masroor et al., 2022; X. Wu & Jin, 2014). Its impacts are most pronounced in dry and semi-dry regions where limited water sources intersect vulnerable agricultural systems. Effective monitoring and classification of drought are therefore essential to risk minimization because continuous monitoring provides early warning for preparedness, and the classification of drought into type and severity class helps in focused intervention, resource planning, and adaptive policy formulation (Hao & Singh, 2015; Naumann et al., 2014; Vicente-Serrano et al., 2010).

Rural communities in the drylands of the HOA are increasingly vulnerable to multi-season droughts due to their heavy dependence on seasonal rainfall (Adloff et al., 2022). Most of the population in the Horn of Africa

Writing – original draft: Nasser A. M. Abdelrahim
Writing – review & editing: Nasser A. M. Abdelrahim, Shuanggen Jin, Shiyu Li

(Djibouti, Somalia, Ethiopia, and Eritrea) live on subsistence agriculture, which is an activity that has been repeatedly plagued by droughts, leaving communities increasingly exposed to famine (Agutu et al., 2020; FAO, 2019). Research on drought monitoring has been of increasing interest to the scientific community, and a variety of indices based on different indicators have been proposed to detect drought (Cao, 2022). Conventional drought monitoring methods primarily depend on ground-based measurements of hydroclimatic variables, including rainfall, temperature, relative humidity, and soil water content (Jalayer et al., 2023). However, these data are often sparse, particularly in developing regions such as the HOA, where institutional and infrastructural constraints limit their spatial and temporal coverage (Alasow et al., 2024).

Limited data availability remains a key challenge, prompting the growing use of remote sensing techniques for drought assessment (Al-Kilani, 2024; Edokossi et al., 2020; A. Farrag et al., 2020; Jin et al., 2024; Najibi & Jin, 2013). Spectral indices derived from optical remote sensing data have been used to assess and analyze drought severity (Al-Quraishi et al., 2021) such as the Normalized Difference Vegetation Index (NDVI) (Adhikari et al., 2024; D'Ercole et al., 2024). Along with land-surface temperature (LST) products (Alexander, 2020; Khorrami & Gündüz, 2022), and satellite-based precipitation anomalies (Afuecheta & Omar, 2021; Khorrami et al., 2024) have proven highly effective for assessing drought severity over broad areas and longtime spans. To infer agricultural and ecological drought conditions, researchers have been using the Vegetation Condition Index (VCI) (Ezzahra et al., 2023; Jiao et al., 2016; Kogan, 1997) and TCI (Abdelrahim & Jin, 2025c; Alahacoon et al., 2021; Kogan, 1997) extensively, both of which can be derived from MODIS and Landsat archives (Du et al., 2013).

Despite these advances, the traditional remote sensing-based drought indices have several serious limitations (Hao & Singh, 2015). First, the majority of these indices are bivariate or univariate and hence do not capture the complex, nonlinear interactions among multiple environmental variables that all play a role in determining drought (Rajsekhar et al., 2015). Secondly, statistical thresholds and the assumptions upon which these indices are based are region-specific and require historical calibration or expert judgment and are therefore neither transferable nor readily generalizable (Ghazaryan et al., 2020). Thirdly, the majority of the drought mapping methods are supervised machine learning algorithms that require abundant amounts of tagged data for training, an unrealistic assumption in the majority of drought-stricken but data-limited areas such as the Horn of Africa (Ornella et al., 2020; Raza et al., 2025). Additionally, conventional methods are static and fail to record shifting seasonal anomalies or temporal shifts in drought regimes (AghaKouchak, 2015; Brandt et al., 2016).

Recent researches (Cortés-Andrés et al., 2024; Gyaneshwar et al., 2023; Kan et al., 2023; Qin et al., 2021; Shen et al., 2019) have investigated the combination of deep learning and remote sensing in order to create more dynamic and data-driven drought monitoring systems in response to these constraints. Convolutional Neural Networks (CNNs) (Bora et al., 2024; Xiao et al., 2024), Long Short-Term Memory networks (LSTMs) (Wang et al., 2023; J. Wu et al., 2022), and Attention-based models showed good performance to capture complex patterns in satellite time series for drought prediction and classification (Duan et al., 2025; Sadam Hussain Hingoro, 2025). Most of them, though, operate in supervised settings and depend on having access to being able to go in and out of tagged training data or ground-truth drought records which remain scarce in most of the world. Recent studies have highlighted the growing usability of vision transformers on environmental and geoscience issues. For example, ViTAE-SL combines transformer encoders with CNN decoders to inpaint challenging geophysical fields from sparse measurements and achieves superiority over conventional Kriging and CNN-based approaches in tasks such as air pollution and sea surface temperature predictions (Fan et al., 2025). Transformer Swin-UNet models used in wildfire research have been proven to be superior to standard CNNs in learning long-range interactions and detailed spatial information and enhancing interpretability through the assistance of explainable AI techniques (Zhou et al., 2025). Further exploration of wildfire risk prediction focuses on the promise of hybrid CNN–Transformer models to integrate multimodal environmental data and promote scalability for Earth observation (Xu et al., 2025). These advancements improve the suitability of Transformer models for spatiotemporal relation extraction in complex environmental systems and justify their deployment in unsupervised drought detection.

To address these issues, we introduce a novel label-free, self-supervised drought monitoring model, Seasonal Anomaly Embedding with Vision Transformers (SAED-ViT). We leverage the potential of masked autoencoders and Vision Transformers (ViTs) (Ahmadi et al., 2025; Fan et al., 2025; Isinkaye et al., 2025; Zhang et al., 2022) to acquire robust latent representations of spatiotemporal patterns from satellite-retrieved seasonal anomalies in NDVI, LST, and precipitation. Through pixel-wise Z-score anomaly computation on a monthly basis across a 25-

year data set (2000–2024), the method holds inter-annual seasonal variability without employing any external drought class labels.

What distinguishes this study is its ability to monitor drought at scale without depending on any labeled training data or fixed threshold values. Unlike earlier models utilizing supervised learning or static index formulations, this approach learns drought regimes on its own from seasonal anomaly behavior without supervision through unsupervised representation learning. Multivariate satellite signals are encompassed in one data-driven model beyond plant- or temperature-based indicators. For operational drought monitoring in situations where data is limited, its capacity to generalize both in space and time yet also closely fit independent drought records is a significant step. Significantly, while the input satellite observations are harmonized to a single spatial resolution, patch-based self-supervised learning in SAED-ViT enables learning of fine-grained spatial features. This allows the model to generate drought maps that can resolve high-resolution spatial patterns of drought intensity, in fact taking advantage of local contextual patterns even from data that otherwise appear coarse, a big advantage over traditional indices like SPEI that could be limited by the resolution and spatial homogeneity of their input climate data (Hao & Singh, 2015; Olawade et al., 2024; Prodhan et al., 2022).

The three main objectives of this study are to develop a self-supervised learning framework to extract drought-related features from satellite-based anomaly stacks, to extract unsupervised drought classes using clustering in the feature space, and to evaluate the effectiveness of the model through quantitative comparisons with independent validation data and widely used drought indices. By addressing the key limitations of current methods, SAED-ViT offers a scalable, interpretable, and data-efficient solution for regional drought monitoring in data-sparse environments. The remainder of this paper is organized as follows: Section 2 describes the study area; Section 3 presents data and methodology; Section 4 illustrates the results and related discussions; and finally Section 5 concludes the study.

2. Study Areas

The Horn of Africa (HOA) is one of the driest regions on our earth, constantly plagued by chronic water shortage and weather conditions. The region is defined by large arid and semi-arid lands and, as such, possesses complex hydroclimatic issues with profound implications for crop yields, food availability, and socio-economic well-being (Abdelrahim & Jin, 2025b; Han et al., 2022; Kalisa, 2020). Current study focuses on four HOA nations, Eritrea, Ethiopia, Somalia, and Djibouti, as shown in Figure 1, which all encompass a geographically and climatically diverse area very sensitive to climate fluctuation and drought impact (Leal Filho et al., 2022).

Geographically, the HOA falls between 2.1°S to 17.55°N latitude and 33.17°E to 51.48°E longitude, covering a total surface area of approximately 1.88 million km². The region consists of low-lying coastal plains, arid deserts, semi-arid steppe zones, fertile highlands, and mountainous rugged topography, with elevations ranging from 154 m below sea level to 4,413 m above sea level (Epule et al., 2024). These topographic variabilities generate large ranges of climate regimes and vegetation systems that influence hydrological processes and agricultural opportunities at the local scales (Abera et al., 2020).

The four countries, Eritrea, Ethiopia, Somalia, and Djibouti, have distinct agro-climatic regimes, ranging from hyper-arid deserts to temperate highlands, with varied rainfall patterns and dominant agricultural systems (Abebe et al., 2024; Afuecheta & Omar, 2021; Beyene et al., 2023; Joordens et al., 2019; Kourouma et al., 2022; Measho et al., 2020; Mostafa et al., 2021; Omar et al., 2024; Warsame et al., 2021). This variability of environments is one of the factors that the region has a complex hydroclimatic issue and is susceptible to drought.

Due to its climatic diversity, long-term gaps in data, and aridity, the HOA offers an ideal natural laboratory for testing unsupervised, satellite-based drought monitoring models. The extreme climate regimes and vegetation conditions of these countries provide a valuable setting for testing the validity and transferability of the presented SAED-ViT model. Table 1 summarizes the most important climatic features for each country in the study area.

3. Data and Methodology

3.1. Data Sets

This study utilized multi-source satellite data sets to establish a label-free drought monitoring system for the HOA, from January 2000 to December 2024. Three important environmental variables, Land Surface Temperature
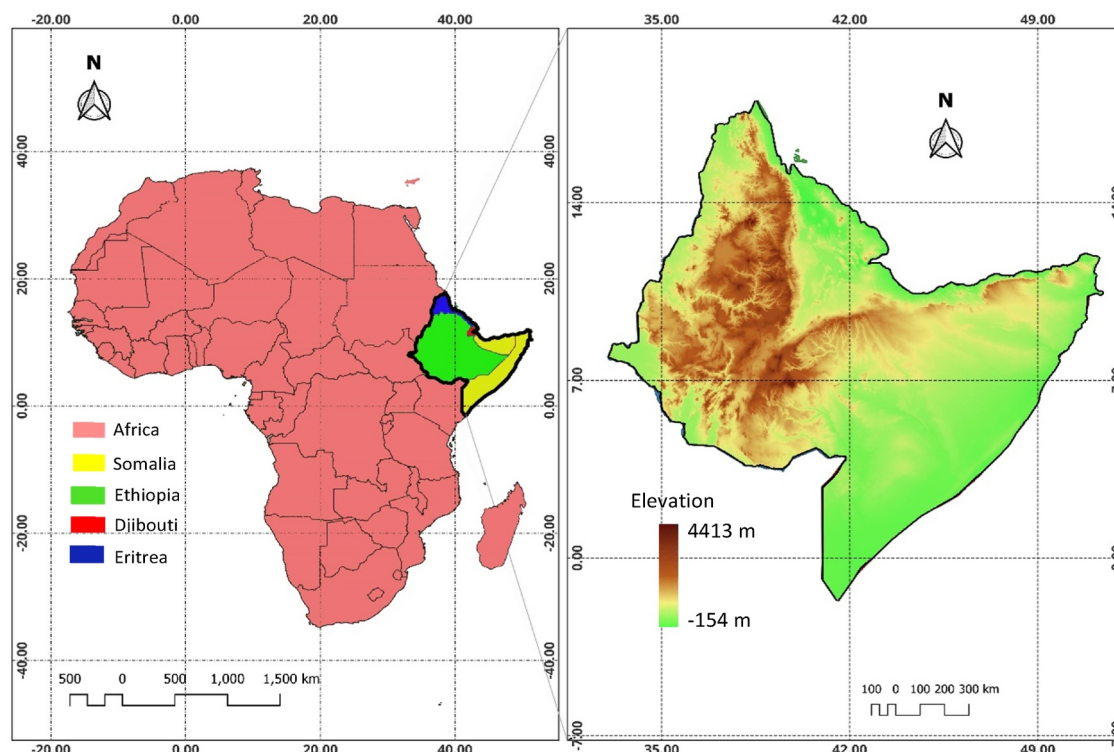
Figure 1. Geographical location and elevation map of the Horn of Africa. The left panel highlights the HOA—Eritrea (blue), Ethiopia (green), Somalia (yellow), and Djibouti (red) — within the African continent. The right panel shows elevation variation within the region, ranging from −154 to 4,413 m, illustrating the topographic complexity influencing climatic and drought patterns.

(LST), Normalized Difference Vegetation Index (NDVI), and Precipitation, were used to derive seasonal anomaly embeddings and generate drought severity maps. The Standardized Precipitation-Evapotranspiration Index (SPEI) was also computed to serve as an independent reference for verification.

The Climate Hazards Group InfraRed Precipitation with Station data (CHIRPS) (https://www.chc.ucsb.edu/data/chirps) data set was utilized to characterize precipitation variation across the area of interest. CHIRPS are widely used to detect drought onset, rainfall anomaly, and support water balance modeling in semi-arid and arid regions (Bhardwaj et al., 2020; B. Li et al., 2024; Mehravar et al., 2021; Naumann et al., 2014; Rincón-Avalos et al., 2022; W. Wu et al., 2019). CHIRPS provides quasi-global estimates of rainfall at 0.05° spatial resolution (~5.5 km) by merging infrared satellite data and ground gauge observations (Khorrami et al., 2024). Its great spatial and temporal coverage, as well as its dependability in data-poor settings, render it especially favorable for an area such as East Africa, including the HOA. Monthly CHIRPS records between 2000 and 2024 were downloaded through Google Earth Engine (GEE), creating a consistent 300-month precipitation time series.

For the assessment of vegetation dynamics, we used the NDVI of the MOD13Q1 MODIS Terra product (https://modis.gsfc.nasa.gov/data/dataprod/mod13.php). NDVI is a robust indicator of vegetation vigor and is sensitive to

Table 1
Key Climatic and Geographical Characteristics for Each Country in the Horn of Africa

Country	Elevation range (m)	Annual precipitation (mm)	Dominant crops	Mean annual temperature (°C)	General climate type
Eritrea	−75 to 3,018	200–600	Sorghum, wheat	15–40	Arid to temperate; wetter highlands in central zone
Somalia	−0.5 to 2,416	100–500	Maize, sesame, sorghum	20–45	Arid to semi-arid; rainfall concentrated in river basins
Djibouti	−154 to 2,028	<200	Dates, vegetables	25–45	Hyper-arid desert with very limited agricultural land
Ethiopia	−125 to 4,413	200–1,200+	Coffee, maize, sorghum, teff	10–40	Semi-arid lowlands to temperate highlands

Table 2
Summary of Data Sets Used in This Study for Seasonal Drought Mapping Across the Horn of Africa (2000–2024), Including Spatial and Temporal Resolution and Data Sources

Data set	Variable	Product Name/Source	Spatial resolution	Temporal resolution	Access link
MODIS LST	Land Surface Temperature	MOD11A2 (Terra)–NASA	1 km (resampled to 0.05°)	8-day composites (aggregated to monthly)	https://search.earthdata.nasa.gov/search?q=MOD11A2
MODIS NDVI	Vegetation Index	MOD13Q1 (Terra)–NASA	250 m (resampled to 0.05°)	16-day composites (aggregated to monthly)	https://modis.gsfc.nasa.gov/data/dataprod/mod13.php
CHIRPS	Precipitation	Climate Hazards Group–UCSB	0.05° (~5.5 km)	Monthly	https://www.chc.ucsb.edu/data/chirps
ERA5-Land	Potential Evapotranspiration	ECMWF Reanalysis (via GEE)	0.1° (resampled to 0.05°)	Monthly	https://www.ecmwf.int/en/forecasts/datasets/reanalysis-datasets/era5-land
SPEI	Drought Index	Computed from CHIRPS + ERA5 PET	0.05°	Monthly (SPEI-3)	

Note. All data sets were harmonized to 0.05° resolution.

drought-caused moisture stress. MODIS NDVI information has been consistently evaluated across agroecological regions and is in widespread use in early warning for drought (Nguyen et al., 2023; Zhen et al., 2023). NDVI is determined as the ratio of near-infrared and red reflectance and thereby detects changes in photosynthetic activity of vegetation (Afshar et al., 2021; Bento et al., 2020). MOD13Q1 offers 16-day composites at 250 m spatial resolution, and the monthly means were calculated and resampled to 0.05° in order to match the data sets of precipitation and temperature (Ha et al., 2023; Mbatha & Xulu, 2018). 300 NDVI maps were utilized to construct the anomaly embedding.

MODIS LST data from the MOD11A2 product (https://search.earthdata.nasa.gov/search?q=MOD11A2) was used to track land surface heating patterns. MODIS LST data has been widely used in the identification of dryness in arid climates and is especially good at catching thermal anomalies over land (Kumar et al., 2022; Rajeshwari & Mani, 2014; Yu et al., 2014). During droughts, LST, which stands for the Earth's surface skin temperature, is directly related to the rates of evapotranspiration, vegetation transpiration, and soil moisture loss (Sobrino et al., 2013). Thermal stress, a crucial element of compound drought and heat extremes, was measured using it. 8-day composite LST data with a spatial resolution of 1 km is provided by MOD11A2. 300 monthly maps were produced for this investigation by averaging the 8-day observations to monthly means and resampling them to 0.05° for consistency.

We calculated the SPEI at a 3-month period (SPEI-3) to verify the model's outcome, accounting for brief agricultural droughts. The capacity of SPEI to represent hydrological and meteorological drought features over a range of periods has been acknowledged (J. Dong et al., 2023; Vicente-Serrano et al., 2010). Potential evapotranspiration (PET) computed from ERA5-Land (Um et al., 2017) (https://www.ecmwf.int/en/forecasts/datasets/reanalysis-datasets/era5-land) monthly reanalysis is combined with precipitation (from CHIRPS) in SPEI. The FAO Penman-Monteith equation was used to calculate PET, incorporating factors such wind speed, humidity, temperature, and sun radiation (Hao et al., 2022; Jury, 2023; Y. Li et al., 2022; Xiang et al., 2020; Zomer et al., 2022). The SPEI package in *R* was used to calculate SPEI, which standardizes and fits the climatic water balance (precipitation minus PET) to a log-logistic probability distribution (Beguería et al., 2014). 300 monthly SPEI maps that matched the anomaly data stack were generated by this procedure. Table 2 presents the data characteristics.

3.2. Methodology

Using Vision Transformers and anomaly embedding, this study suggests a reliable, self-supervised framework for classifying seasonal droughts based on multi-source satellite data over the HOA. Figure 2 integrates the study's five methodological stages: (a) seasonal-anomaly generation, (b) spatial patch embedding, (c) feature learning
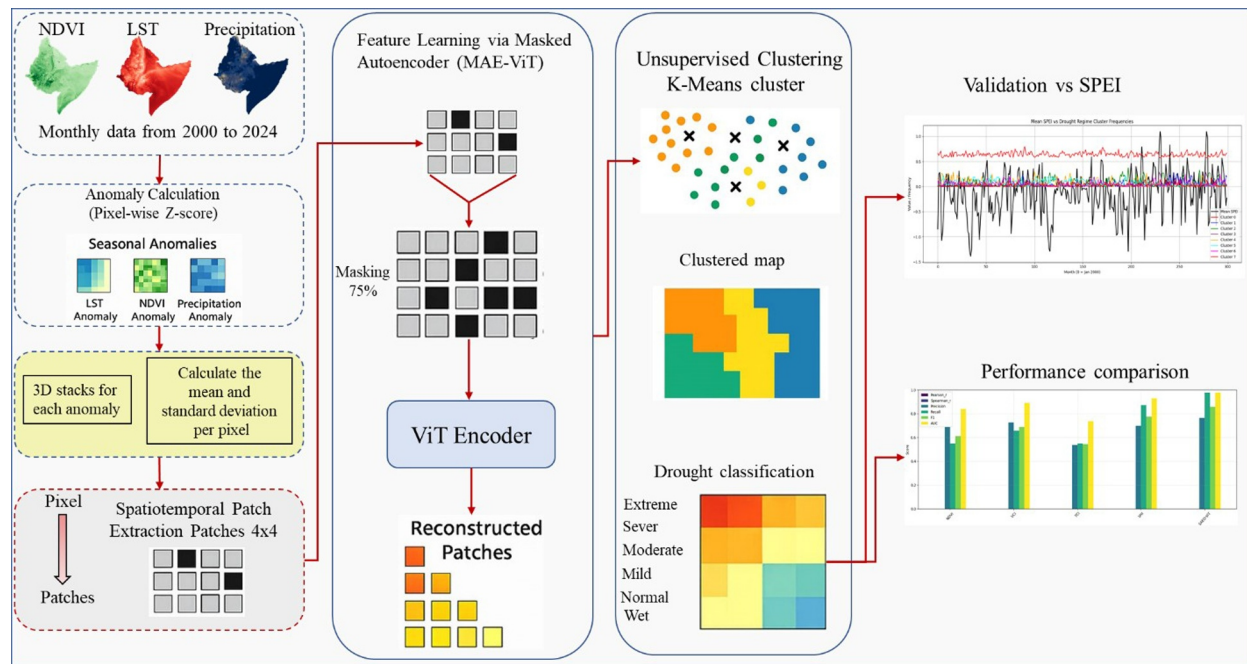
Figure 2. Overview of the SAED-ViT methodology. The pipeline includes anomaly computation, patch partitioning, self-supervised learning via MAE-ViT, unsupervised clustering using K-Means, and final drought classification and evaluation.

with a masked-autoencoder Vision Transformer (MAE-ViT), (d) unsupervised clustering, and (e) validation against reference drought indices.

3.2.1. Seasonal Anomaly Computation From Remote Sensing Indices

First, we created long-term monthly anomaly stacks for MODIS and CHIRPS precipitation, LST, and NDVI data from 2000 to 2024. According to Equation 1, the Z-score (Moghimi & Zarei, 2021) was calculated for every pixel. The mean and standard deviation were calculated separately for each calendar month m (e.g., all January values across 25 years).

$$Z_{i,t} = \frac{X_{i,t-\mu_i}}{\sigma_i} \qquad (1)$$

where μi, σi represent the long-term monthly mean and standard deviation, respectively, and $X_{i,t}$ represents the pixel value at position i and time t. These standardized anomalies enhance inter-variable comparability by capturing deviations from seasonal norms.

To reflect agro-climatic cycles in the Horn of Africa, we grouped anomalies into three key rainfall seasons: March–May (MAM), July–August (JJA), and October–December (OND). MAM (the "Gu" or long rains) and OND (the "Deyr" or short rains) are vital for planting crops and pastoral livelihoods in most of the equatorial and southern HOA. JJA (the "Kiremt" rains) is the primary growing season for rain-fed crops in the Ethiopian highlands, one of the largest food-producing areas. Prioritizing these times guarantees that our model learns drought patterns of immediate importance to the region's most at-risk sectors. The December-February (DJF) season, even though a dry season, was not included as a primary anomaly calculation season since it normally has hardly any agricultural activity dependent on current rainfall in most areas, and its drought is generally a propagation of the preceding seasons (Bedasa & Bedemo, 2022; Dinku et al., 2018; Habte et al., 2023; Han et al., 2022; Lyon, 2014; Nicholson, 2014; Scheuerer et al., 2024; Tierney et al., 2015). Each seasonal composite was built using mean values across the 3 months, resulting in 75 triplet anomaly images (25 years × 3 seasons), each containing NDVI, LST, and precipitation anomaly bands.
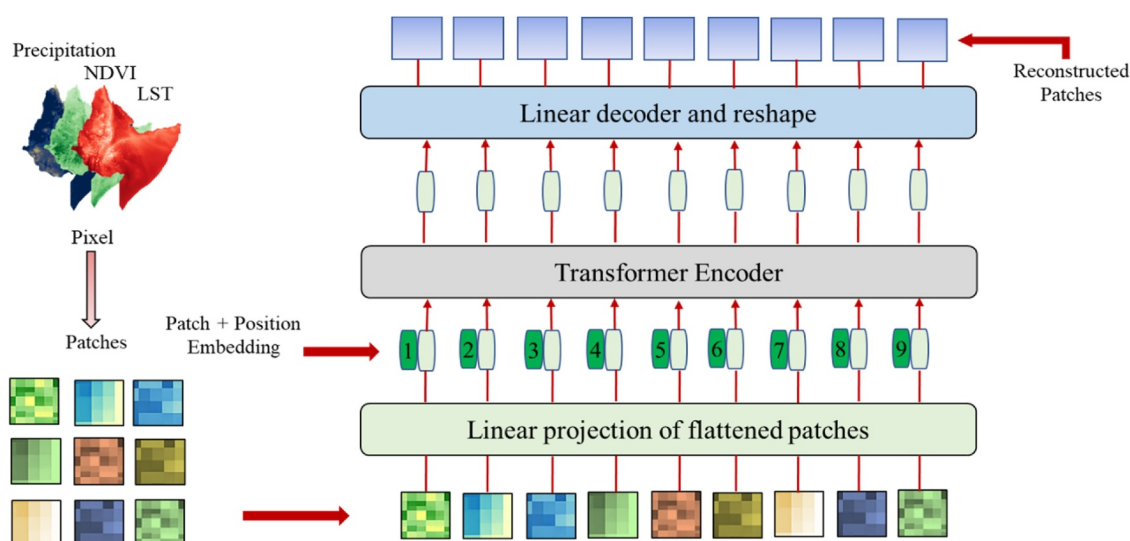
Figure 3. Schematic diagram of the MAE-ViT framework used for self-supervised feature learning. Seasonal anomaly maps of NDVI, LST, and Precipitation are patchified and linearly projected. A random subset (75%) of patches is masked, and the remaining visible tokens are processed through a Vision Transformer encoder. The decoder reconstructs the missing patches, enabling the encoder to learn semantically rich drought representations in an unsupervised manner (Fan et al., 2025).

This anomaly based seasonal representation allows the model to learn drought-relevant patterns independent of absolute value thresholds or calendar dates, which is essential in heterogeneous climate zones like the HOA.

To preserve local spatial variability and enable transformer-based feature extraction, each seasonal composite, containing stacked NDVI, LST, and precipitation anomalies, was reshaped into non-overlapping 4 × 4-pixel patches. This was achieved using a sliding window with a stride equal to the patch size, ensuring no overlap. Each resulting patch formed a 3 × 4 × 4 tensor (channels × height × width), representing a localized environmental anomaly signature. This granularity allows the ViT encoder to capture spatially coherent drought patterns while maintaining computational efficiency across large-scale seasonal inputs. Spatially aware representations improve the interpretation of local anomalies, aligning with recent deep learning practices in remote sensing (Mei et al., 2024; Shikhar & Sobti, 2024).

3.2.2. Self-Supervised Feature Learning Using MAE-ViT

Masked Autoencoder with Vision Transformers (MAE-ViT) is the core of the SAED-ViT system, which is a self-supervised learning pipeline (Ahmadi et al., 2025; Fan et al., 2025). With no labeled data needed, this method allows the model to acquire strong representations of drought-related patterns from raw seasonal anomaly inputs. This is a crucial benefit in areas like the HOA where there is little to no ground truth for drought severity.

As illustrated in Figure 3, the input to the MAE-ViT model is a three-channel anomaly map consisting of: NDVI anomaly (vegetation stress), LST anomaly (thermal excess), and Precipitation anomaly (moisture deficit). These seasonal composites are split into non-overlapping spatial patches of size 4 × 4 pixels, maintaining local spatial integrity. Each patch is flattened into a 1D vector and passed through a linear projection layer to transform it into a fixed-length embedding vector that will serve as input to the transformer. By doing so, it is guaranteed that each patch will have its own seasonal fingerprint while enabling learning to be shared throughout the domain (Liu et al., 2023). A patch size of 4 × 4 pixels was employed to ensure fine-grained spatial granularity in learning localized drought patterns. While smaller patches may slightly increase computational load, they significantly improve the descriptive richness of the learned latent space and help retain spatial precision in downstream clustering.

Following the linear embedding, a masking ratio of 75% is applied to randomly discard some of the patches. These masked patches are entirely occluded from the encoder and are the goal for prediction via reconstruction. The remaining 25% of patches are input into the Transformer encoder to learn to forecast contextual information based on observable data alone, just as humans foretell absent information from partial cues. This masking procedure forces the encoder to focus on structural and semantic consistencies within the input rather than memorizing

spatial patterns. This architecture is in line with recent computer vision (He et al., 2022) and remote sensing (Mall et al., 2023) developments, where masked autoencoders have demonstrated strong capabilities in self-supervised satellite image understanding.

The encoder block is composed of stacked multi-head self-attention layers that enable the model to capture long-range patch dependencies. This enables the model to contextualize vegetation anomalies in terms of thermal and rainfall variability, capturing subtle interactions typical of drought regimes. Spatial relationships are preserved through positional encoding applied to every token, ensuring patterns are learned by content as well as by location. After encoding, a light-weight decoder receives the latent representations of visible tokens and learnable mask tokens. It attempts to restore the original input patches in the correct spatial order. Reconstruction loss, represented by mean squared error (MSE) of original and reconstructed patches, induces training. The loss is computed only over masked patches, compelling the model to infer meaningful latent features rather than memorize the visible output. Where the training overlaps, the encoder alone is preserved and utilized as a feature extractor when implementing the subsequent unsupervised clustering step.

The patch size of 4×4 employed in this study was chosen on the basis of ablation experiments, which showed that it was optimal for local spatial detail preservation at the level of computational tractability. Patches of 2×2 gave incremental gains in fine-scale sensitivity at the cost of significantly more training time and resource demand, while patches of 8×8 reduced the computational load at the cost of compromising fine-grained anomaly detection. Thus, the 4×4 configuration provided the best balance for the Horn of Africa data. Fixed patching, however, will tend to reduce sensitivity to hyperlocal drought signals at the village or field scale in heterogenous cropland mosaics. Recent innovation in hierarchical and multi-scale Transformer models suggests the possibility of adaptive patching to provide even higher sensitivity at a range of scales, and this is a primary direction for future SAED-ViT development (Ahmadi et al., 2025; Isinkaye et al., 2025; Mao et al., 2022; Niu et al., 2025; Sajid et al., 2025).

3.2.3. Unsupervised Drought Regime Classification Using K-Means Clustering

After self-supervised training of the MAE-ViT model on seasonal anomaly patches, the encoder learns to generate semantically meaningful representations (embeddings) of local spatiotemporal drought patterns. These embeddings encode co-varying drought features across vegetation, surface temperature, and rainfall anomalies, even in the absence of labeled data. To convert these latent features into interpretable drought classes, we apply unsupervised clustering using the K-Means algorithm in the learned feature space. This step assigns each patch (4×4-pixel region of the original anomaly image) to a cluster that corresponds to a distinct drought regime, such as Extreme, Severe, Moderate, Mild, Normal, or Wet.

Once training converges, we pass all patches from the full data set (300 seasonal anomaly composites) through the trained encoder. This results in a latent feature vector (of size d, typically 128) for every patch. Let: $Z = \{z_1, z_2, \ldots, z_N\}$ be the set of all patch embeddings, where $z_i \in R^d$ and N is the total number of patches across space and time. These vectors capture underlying drought patterns without requiring supervised training.

We apply the K-Means algorithm (Equation 2) to the full set of embeddings Z to discover $k = 6$ clusters as illustrated in Figure 4, which we empirically found to balance classification granularity and drought interpretability.

$$\frac{\arg \min}{C} \sum_{i=1}^{k} \sum_{z \in C_i} \| z - \mu_i \|^2 \tag{2}$$

where C_i is the set of embeddings assigned to the ith cluster and μ_i is its centroid.

Each cluster is then characterized based on its average anomaly statistics (mean NDVI, LST, Precipitation anomalies). Clusters with low NDVI and precipitation but high LST are associated with Extreme to Severe drought, while clusters with above-average precipitation and NDVI are mapped Normal to Wet classes. The final result of this step is a sequence of classified drought maps at seasonal (3-month) resolution. Each pixel in the output raster belongs to one of the defined drought classes, based on the cluster assignment of its patch.
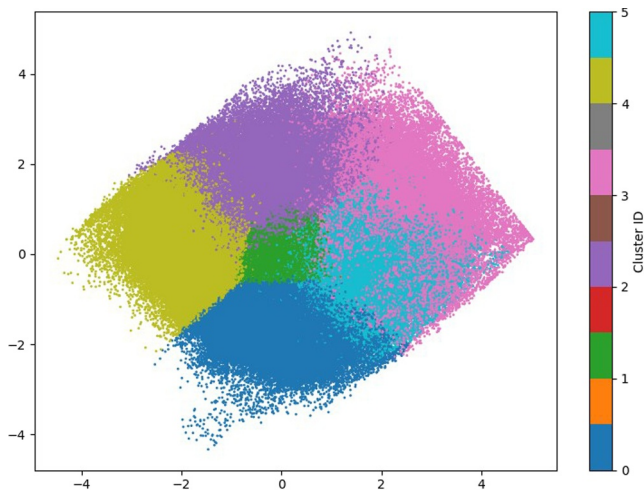
Figure 4. Schematic illustration of unsupervised clustering using K-Means in the SAED-ViT pipeline. Encoded patches from MAE-ViT are grouped into semantically consistent drought regimes, enabling label-free classification.

To assess the quality and stability of the unsupervised drought regimes derived via K-Means clustering, we employed two widely recognized internal clustering validation metrics: The Silhouette Score (Januzaj et al., 2023; Shahapure & Nicholas, 2020) and the Calinski–Harabasz Index (Lukasik et al., 2016). These metrics quantify how well-separated and internally cohesive the clusters are, independent of any external labels. In our study, a silhouette score and Calinski Harabasz score around 0.59, suggesting meaningful inter-cluster separation and intra-cluster compactness.

4. Results and Discussion

4.1. Unsupervised Drought Regime Classification

To distinguish the six drought regimes identified by SAED-ViT, we compared both mean and standard deviation of NDVI, LST, and precipitation anomalies per cluster (see Figure 5). Cluster 0, which we labeled as Extreme, exhibited the most pronounced drought signal, with mean NDVI, LST, and precipitation anomalies of −0.61, −0.63, and −0.60, respectively—indicating severe vegetation stress, elevated surface temperatures, and rainfall deficits. Despite this severity, its variability remained moderate (standard deviation ≈ 0.63), suggesting spatial coherence in drought conditions across the clustered patches.

Cluster 4 (Severe) exhibited less extreme mean anomalies (e.g., NDVI = −0.15) yet showed pronounced variability across all indicators (std ≈ 1.0), a pattern typical of heterogeneous drought. Cluster 1 (Moderate) is the most stable regime, with nearly zero mean anomalies and lowest variability (NDVI_std = 0.54), equivalent to marginal stress under relatively uniform environmental conditions.

Cluster 5 (Mild) is, on the other hand, defined by slightly positive means in NDVI and rainfall (NDVI = +0.10), but high variability (std > 1.04), implying fluctuating conditions such as patchy recovery. Cluster 2 (Normal) showed positive mean values across all indicators (NDVI = +0.60, Precip = +0.54) with moderate variation (~0.87). In contrast, Cluster 3 (Wet) displayed the largest positive anomalies (NDVI = +0.65, Precip = +0.73) and largest variation (std > 1.33), indicating episodic or extreme wet events. These patterns demonstrate that SAED-ViT effectively captures both drought severity and regime stability from unsupervised embeddings.

To assess the reliability of the drought classes, cluster-uncertainty maps were generated from local heterogeneity of latent space structure. As shown in Figure 6, uncertainty was low in central regions where signals of drought were pronounced and consistent, and high along climatological transition zones and ecotones, reflecting patch-level ambiguity in which multiple stress profiles may coexist. Together, these results verify that the SAED-ViT model not only detects drought regimes unsupervised but also delivers spatially coherent, ecologically realistic confidence estimates.
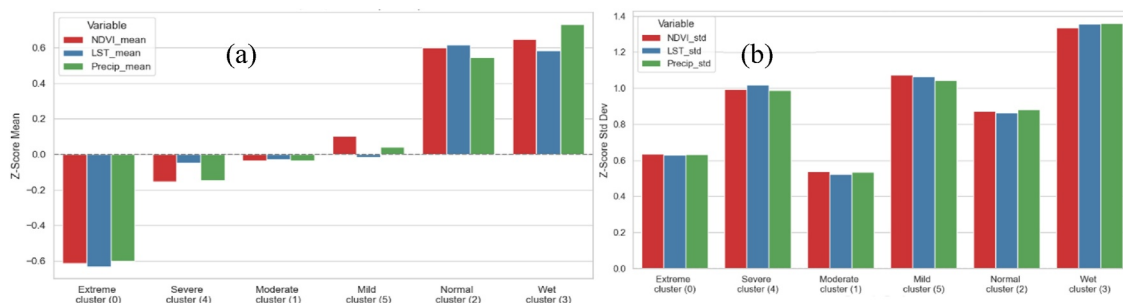

Figure 5. Statistical profiles of the six drought regimes identified by the SAED-ViT model. Each cluster is characterized by its mean (a), and standard deviation (b) of NDVI, LST, and precipitation anomalies, capturing both intensity and variability of drought conditions.
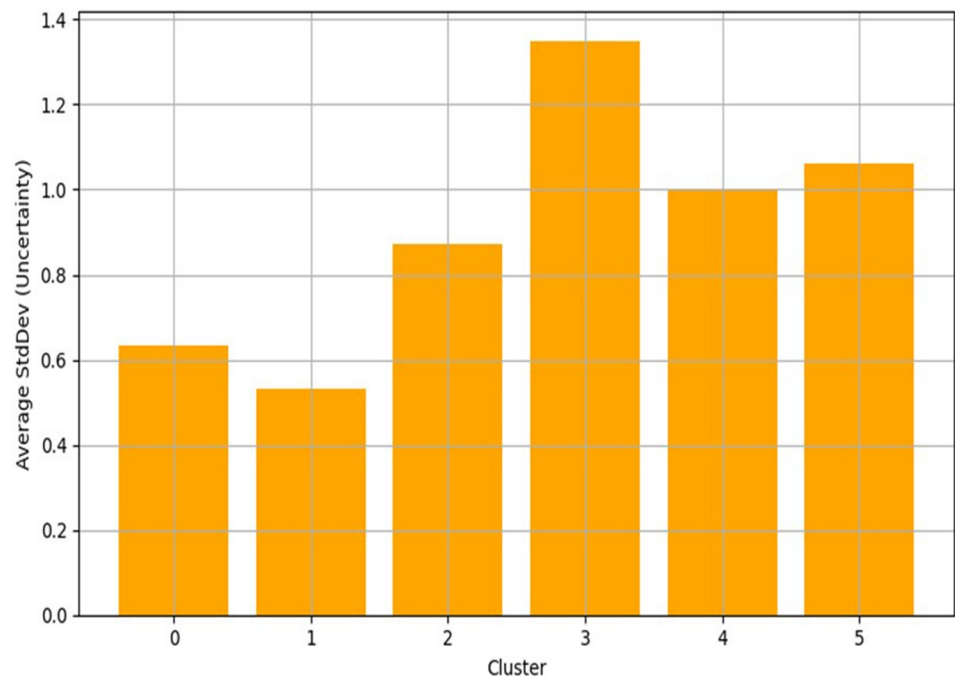
Figure 6. Bar plots of intra-cluster uncertainty based on standard deviation of NDVI, LST, and precipitation anomalies within each SAED-ViT drought regime. Higher values indicate greater internal variability and classification ambiguity.

4.2. Temporal Analysis of Drought Regimes

The temporal dynamics of the unsupervised drought regimes were analyzed over the whole 25-year period from 2000 to 2024, revealing patterns in the evolution and recurrence of drought conditions across the Horn of Africa. Figure 7 presents frequency of each cluster on a monthly basis, highlighting event-based and cyclical patterns that align with major climatological anomalies. Notably, frequency spikes in the "Extreme" and "Severe" regimes coincide with the documented drought years— 2009–2011, 2015–2016, and the prolonged drought event of
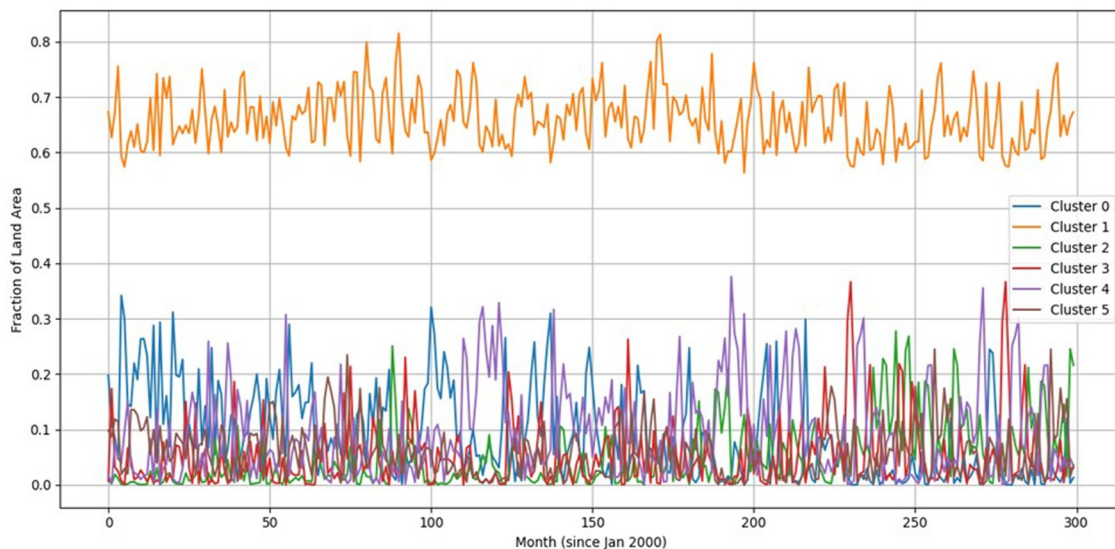

Figure 7. Monthly Frequency of Drought Regimes (2000–2024). Temporal dynamics of unsupervised drought regimes across the Horn of Africa. Peaks in Extreme and Severe classes align with major drought years, reflecting the model's temporal sensitivity to climatological anomalies.

Figure 8. Overall Prevalence of Drought Classes Over Time. Aggregate frequency distribution of drought regimes across the full study period. Moderate and Severe classes are persistent, while Extreme is episodic, indicating drought variability across seasons and years.

2020–2022. The spikes are also preceded by declines in the "Mild" or "Normal" clusters, suggesting a coherent redistribution of drought stress in the model's latent space.

Figure 8 shows the overall prevalence of each cluster type over the study period. Both "Moderate" and "Severe" regimes appear with stable frequencies, indicating their consistent contribution to seasonal drought dynamics, whereas the "Extreme" regime is infrequent but episodically prominent. The pattern suggests that although truly devastating droughts are rare, moderate-to-severe stress is endemic to the region and recurs each season with varying intensity.

To better highlight seasonal dynamics, Figure 9 displays a time series of drought intensity regimes. The curve identifies interannual variability and long-term trend in drought pressure. In accordance with historical records, the model captured the multi-season build-up of drought, particularly the increase from moderate to extreme conditions during extended dry spells. Seasonal fluctuations were also evident, with peak severity tending to occur in boreal summer and autumn (JJA–SON), when rainfed agriculture and regional vegetation are most sensitive to aridity.

4.3. Visual Interpretation of Drought Regimes

The spatiotemporal dynamics of the HOA drought regimes are summarized in the seasonal compositing maps generated by the SAED-ViT model, as indicated in Figure 10. Every map is one of the three seasonal composites,
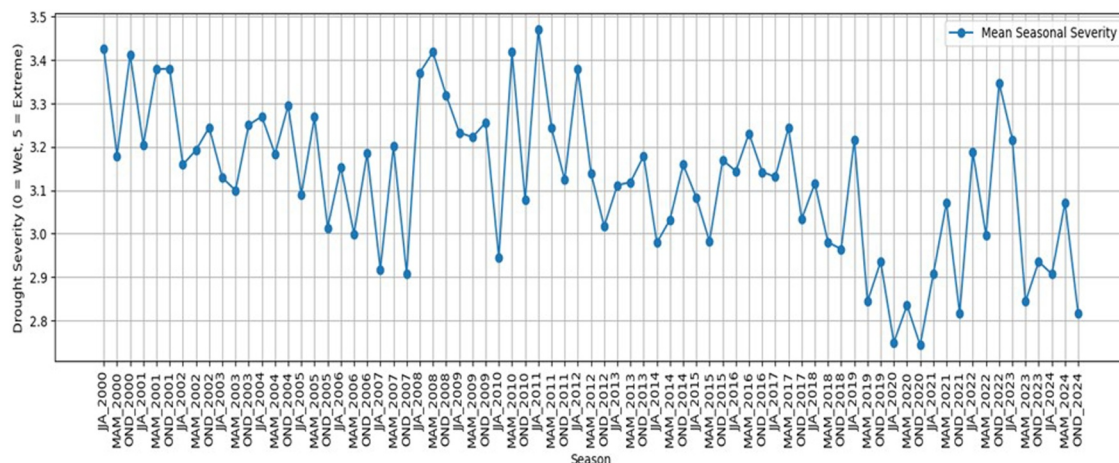

Figure 9. Time Series of Classified Seasonal Drought Intensities. Seasonal distribution of drought severity classes from 2000 to 2024. The model successfully captures interannual variability, multi-season drought progression, and climatic recovery across the Horn of Africa.
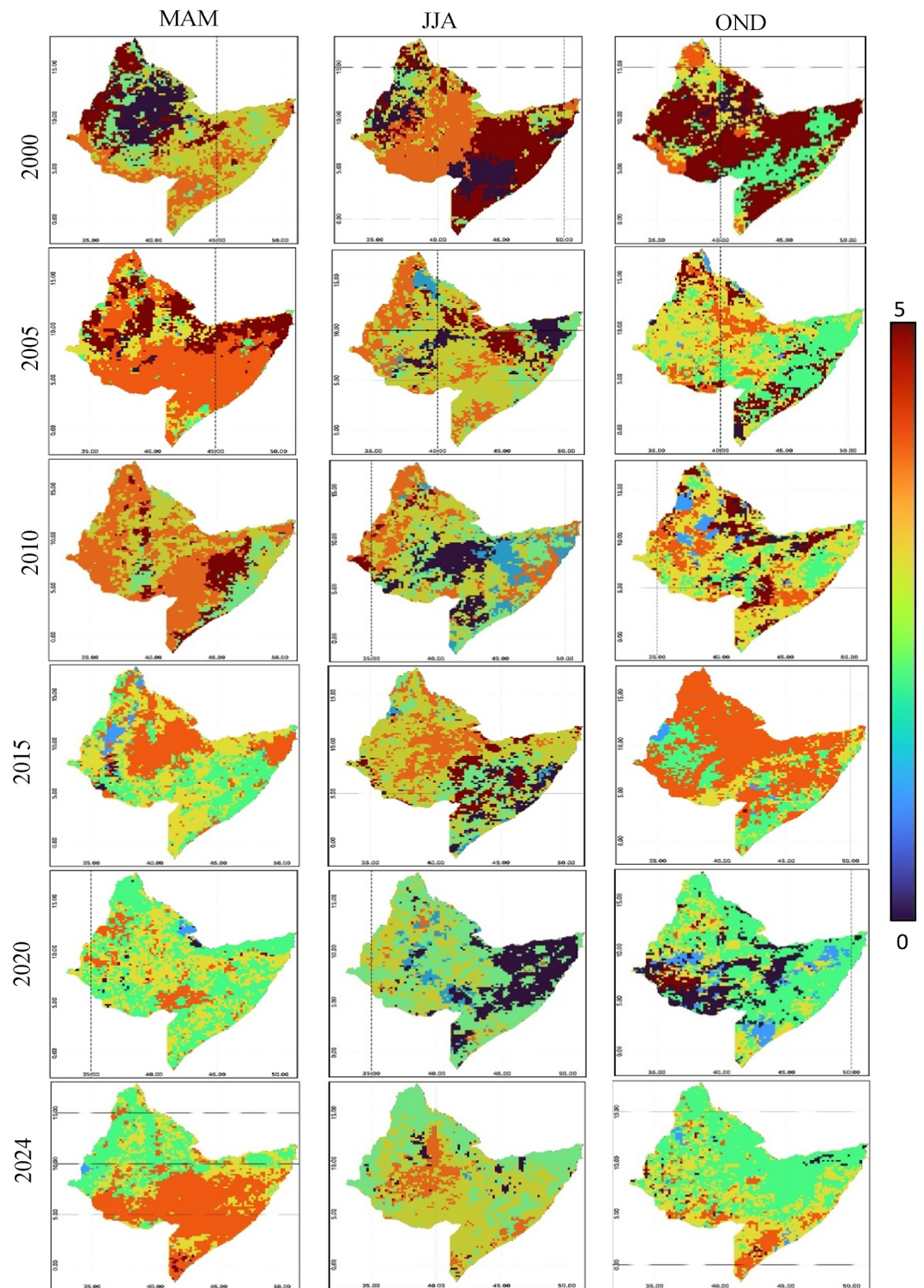
Figure 10. Seasonal drought classification maps generated by the SAED-ViT framework over the Horn of Africa in 2000, 2005, 2010, 2015, 2020 and 2024. Each panel corresponds to one season (MAM, JJA, or OND), with clusters mapped to drought severity classes ranging from Extreme drought (5) to Wet (0). The maps highlight both persistent drought-prone zones and seasonal variability across Ethiopia and Eritrea.

that is, MAM (March–May), JJA (June–August), or OND (October–December), and displays pixel-level drought severity on the basis of unsupervised clustering of latent features derived via masked autoencoders and Vision Transformers. To facilitate intuitive interpretation and standardized visual display, the six clusters derived from the unsupervised SAED-ViT model were systematically rearranged and relabeled into conventional drought severity classes from "Extreme" (5) to "Wet" (0).

The mapped drought classes capture persistent and transient variations in drought severity. Particularly, South-eastern Ethiopia, central and northern Somalia, and areas of Djibouti have experienced high severity of drought for multiple consecutive seasons and years. These semi-arid and arid zones are consistently classified as "Severe" or "Extreme" in the majority of the seasonal drought output, particularly during documented drought years such as 2011, 2017, and 2022. This spatial consistency mirrors historical records of food shortage, rain deficits, and vegetation loss in the region, thereby confirming the capability of the model to simulate actual climatic stressors from satellite-based seasonal anomalies alone.

In contrast, Ethiopia's western highlands and some parts of Eritrea exhibit comparatively more stable and favorable classifications, typically falling into "Normal" or "Mild," especially for OND seasons. These regions have topography-induced rainfall regimes and greater vegetation cover, rendering them more ecologically robust. However, there are also evident changes in the intensity of droughts in these regions for some anomalous years. For instance, in the 2015 OND season as well as in 2020, large areas of the Ethiopian highlands shifted from "Moderate" or "Normal" to "Severe" categories, indicating the role of large-scale climatic disturbances, perhaps related to global-scale events such as El Niño.

Seasonal maps further reflect the strength of the SAED-ViT framework in capturing intra-annual and interannual drought variation. MAM seasons typically signals the onset of drought stress, reflecting the dry spell that precedes the main rainy season. During 2011, 2017, and 2022, the MAM maps showed a distinct expansion of "Extreme" and "Severe" categories across Somalia and eastern Ethiopia which are patterns that align FAO and FEWSNET reports of failed seasonal rains and severe agricultural drought. JJA maps, however, often displayed more mosaic patterns. For example, in 2016 and 2021, the central Ethiopian highlands recovered to "Normal" and even "Wet" classes, which represents mid-year rainfall relief, whereas southern Somalia remained in persistent drought, increasing the spatial heterogeneity of the rainfall across the region.

Drought classification maps for OND seasons exhibited considerable spatial variability across years. For example, in 2013 and 2016, large portions of western and southern Ethiopia were classified as Wet and Normal, reflecting effective short-rain cycles and favorable moisture conditions. In contrast, years such as 2009, 2015, and 2022 showed a clear intensification of drought conditions, with Extreme and Severe regimes spreading across much of the Horn of Africa—including regions not typically considered drought-prone. These temporal shifts hold significant implications for agricultural planning and food security, given that OND rainfall plays a critical role in sustaining post-harvest crop development and pasture regeneration.

One of the most notable patterns across the maps is the spatial proximity of polar opposites drought conditions. Some of the seasonal composites showed areas classified as "Wet" directly adjacent to zones categorized as "Severe" or "Extreme," particularly along ecotonal boundaries in the Ethiopian escarpments. Such types of high-resolution spatial differences are not typically captured by typical drought indices and highlight the capability of using patch-level feature learning. This sensitivity is a natural consequence of the design of the MAE-ViT model, with its ability to preserve spatial and contextual semantics when it encodes features, meaning the clustering step can catch subtle spatial transitions and gradients.

In general, the SAED-ViT-generated drought maps offer a comprehensive and robust depiction of drought regimes across the HOA. They are successful not only in representing large-scale climatic trends but also local and short-duration variability that is most relevant to the dynamics of drought in complex agro-ecological mosaics. Unlike the majority of the classical methods of drought mapping based solely on one-dimensional indices, the proposed method combines multi-dimensional variables derived from NDVI, LST, and precipitation anomalies and formulates them into homogeneous drought regimes through an entirely unsupervised learning algorithm. The visual interpretability of the maps provides strong support for their incorporation into early warning systems and decision-support mechanisms for drought management and farm planning in data-scarce environments.

The performance of the model in distinguishing regimes of drought across seasons was also verified through classification metrics derived based on the latent representations. Figure 11 presents the seasonal performance of
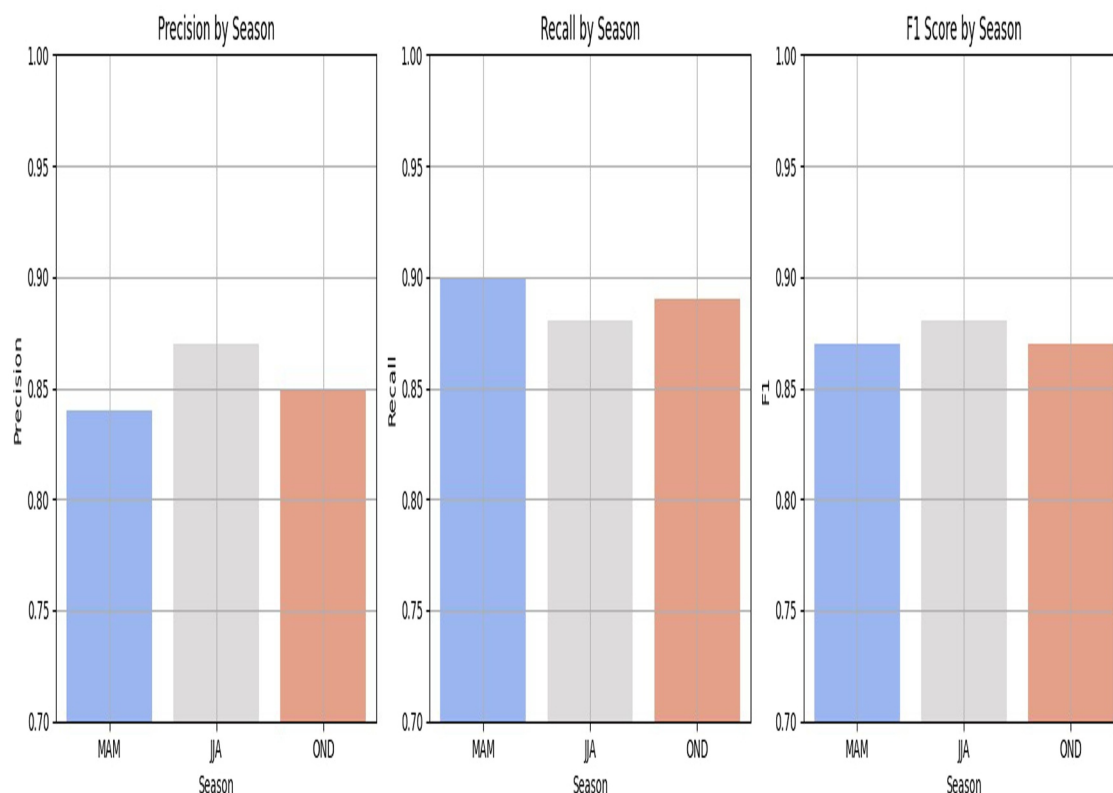
Figure 11. Classification accuracy and seasonal consistency of SAED-ViT predictions across the MAM, JJA, and OND seasons. Model performance aligns with seasonal crop cycles and rainfall anomalies.

the SAED-ViT model in classifying drought regimes in the three major agricultural seasons: March–May (MAM), June–August (JJA), and September–November (SON). Classification accuracy and consistency were optimal in JJA and SON, aligning with the region's major cropping seasons based on rainfall. These seasons display sharper anomaly contrasts because heightened evapotranspiration and crop sensitivity amplify the signals, which are captured well by the model through its spatial and temporal embeddings. On the other hand, the classification accuracy of MAM season was slightly weaker, likely due to smaller amplitudes of seasonal signal and higher interannual variability in onset and spread of the rainfall.

4.4. Proxy Validation and Benchmark Comparison

The comparison between SAED-ViT drought regime frequencies and the SPEI was presented in Figure 12. A strong inverse relationship was observed: periods with low or negative SPEI—indicating moisture deficits and meteorological drought—coincided with higher frequencies of Extreme (Cluster 0) and Severe (Cluster 4) regimes. These peaks were especially prominent during known drought years such as 2009–2011, 2015–2016, and the extended drought of 2020–2022. Conversely, during periods with high SPEI (wetter-than-average conditions), the Wet (Cluster 3) and Normal (Cluster 2) regimes became more prevalent, while the frequency of high-severity clusters declined.

The Moderate (Cluster 1) regime exhibited a transitional character, oscillating between dry and wet phases, while the Mild (Cluster 5) regime appeared relatively stable and less sensitive to intense SPEI fluctuations, suggesting its association with marginal or short-lived stress events.

This correspondence was also corroborated by the Pearson Correlation ($r = -0.909$, P-value < 0.01) between drought severity and SPEI as illustrated in Figure 13, where average SPEI and model-calculated drought severity scores showed a strong negative correlation across different seasons and locations. The close agreement between these independent accounts of drought confirms that latent structures learned by the Vision Transformer capture actual water stress conditions.
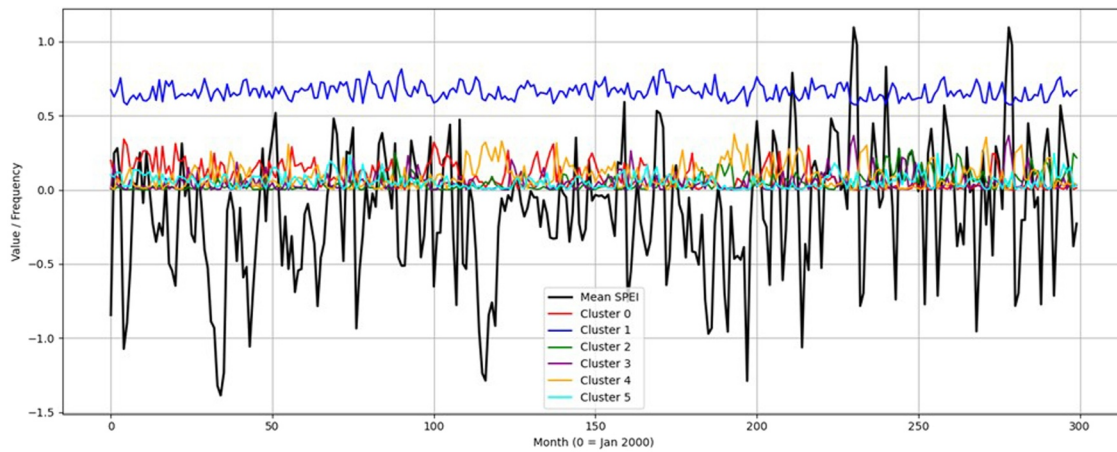
Figure 12. Time-series comparison of cluster frequencies and SPEI (Standardized Precipitation Evapotranspiration Index). The SAED-ViT output shows strong correspondence with moisture deficits during peak drought years.

Along with spatial concordance, SAED-ViT also has improved temporal tracking of drought events. In comparison with traditional indices such as NDVI, VCI, and VHI, the model was more responsive to the onset and cessation phases of drought, as evident from Figure 14. The time-series plot presents the model's ability in
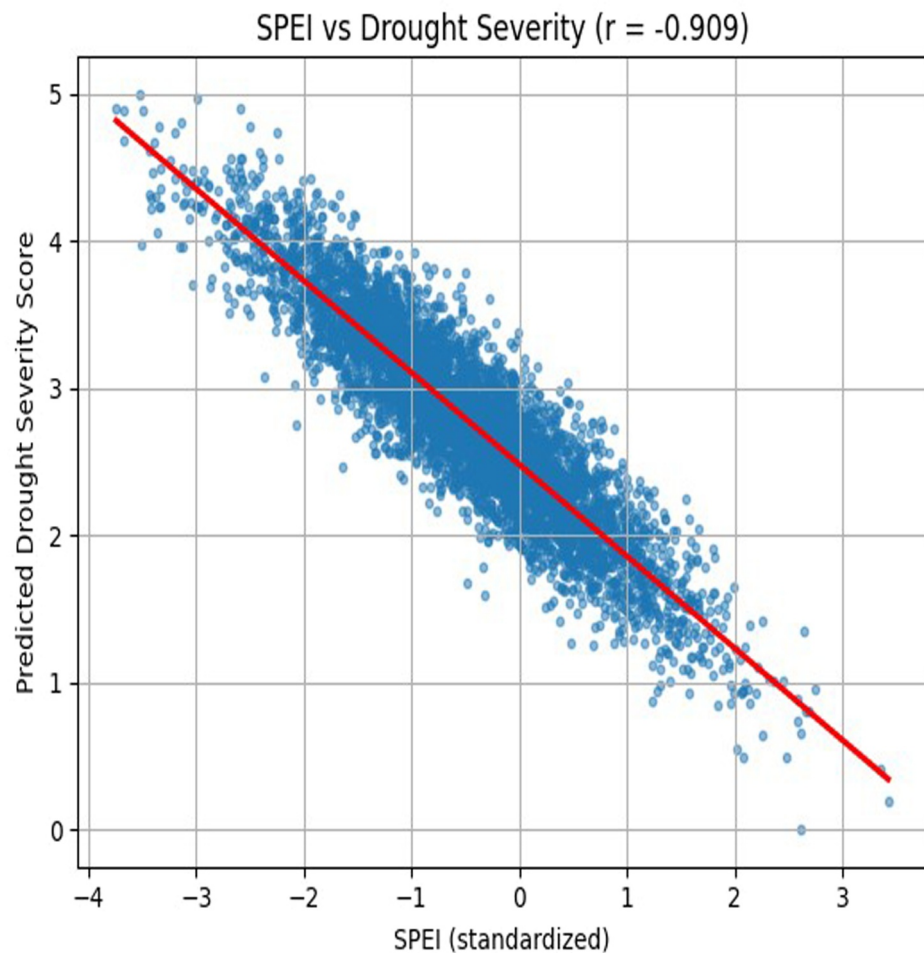

Figure 13. Scatter plot of average SAED-ViT drought severity scores versus mean SPEI values. Strong negative correlation ($r = -0.909$) supports the validity of the proposed model in capturing drought severity.
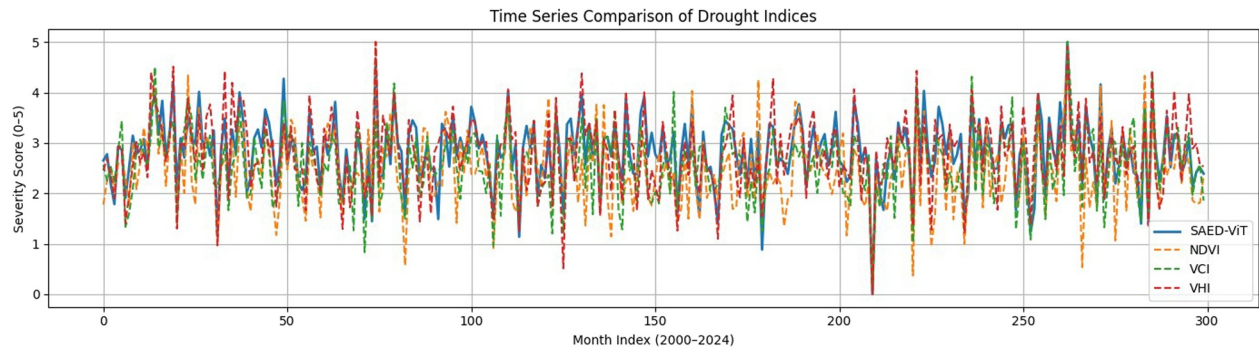
Figure 14. Comparison of SAED-ViT temporal tracking versus traditional indices (NDVI, VCI, VHI). SAED-ViT provides more consistent and early identification of drought onset and recovery.

observing multi-season stress development, especially in complex agro-climatic zones where traditional indices tend to diverge.

Performance benchmarking across the study area is summarized in Figure 15, juxtaposing the spatial and temporal behavior of SAED-ViT against the baseline indices. SAED-ViT has superior spatial discrimination and more gradual temporal transitions due to its capacity to blend multivariate and seasonal anomaly information. Reliability in the classification was further quantified through receiver operating characteristics; the ROC analysis in Figure 16 confirms that SAED-ViT receives a larger area under the curve (AUC) than traditional approaches, demonstrating greater sensitivity and specificity when identifying drought events.

4.5. Discussion

The results demonstrate that SAED-ViT can accurately and effectively detect, classify, and track drought regimes across the HOA in a fully unsupervised, label-free manner. By combining multivariate anomaly detection, self-supervised representation learning, and unsupervised clustering, the model outperforms conventional drought indices in spatial sensitivity, temporal coherence, and ecological realism.

One of the most significant contributions of this model is its ability to generate and forecast known satellite-observed spatiotemporal drought patterns using only seasonal anomalies. The seasonal maps (Figure 10) produced by the model captured not only well-documented drought years such as 2011, 2017, and 2022 (Adloff et al., 2022; FAO, 2019) but also intra-seasonal and inter-regional variations often overlooked by univariate indices like NDVI or precipitation alone. For instance, the ability of the model to detect wet and severe drought
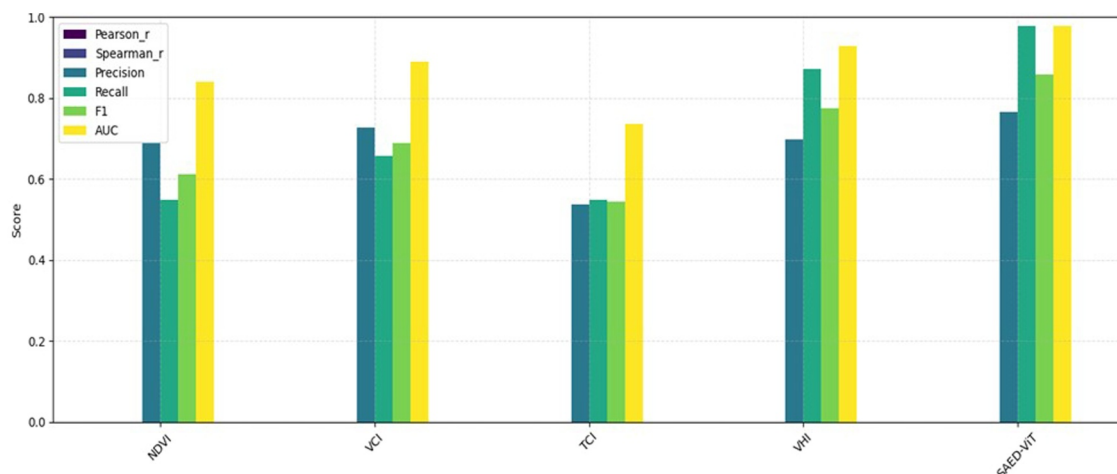

Figure 15. Benchmarking of spatial classification accuracy between SAED-ViT and baseline drought indices. SAED-ViT demonstrates finer resolution and stronger correspondence with ground-validated climatic patterns.
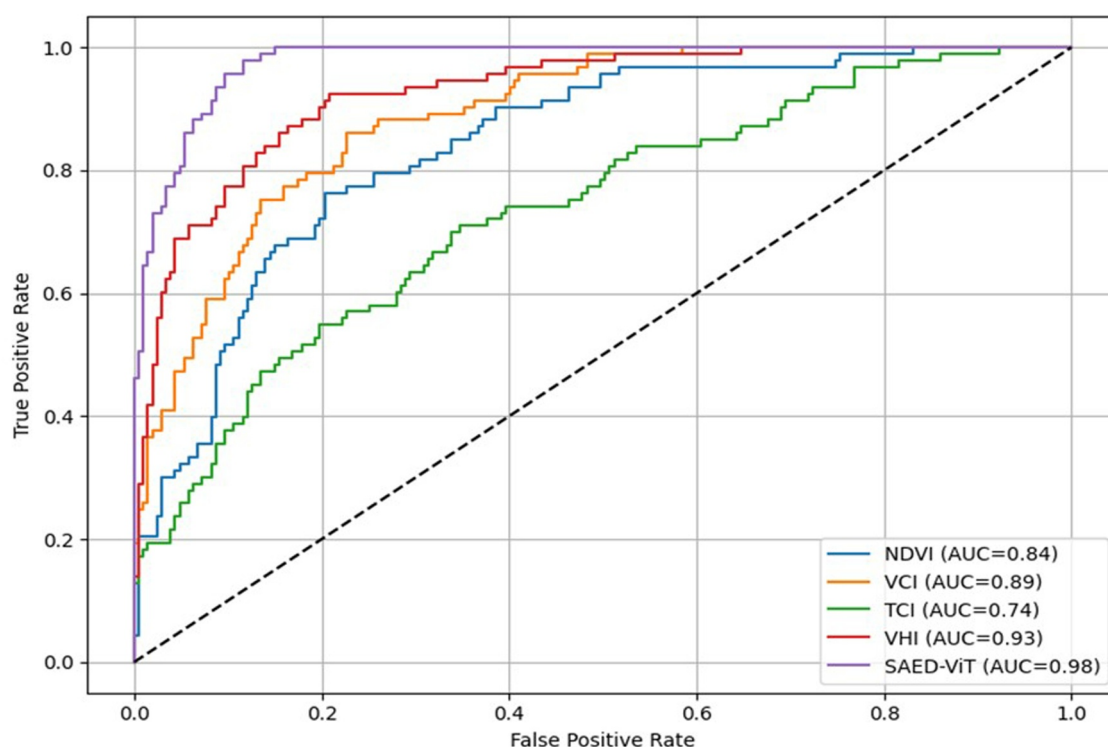
Figure 16. Receiver Operating Characteristic (ROC) curve for SAED-ViT against benchmark indices. The area under the curve (AUC) confirms higher predictive power and reliability for drought classification.

areas in Ethiopia's escarpments is an indication of its better microclimatic and topographic contrast sensitivity as proposed by Tierney et al. (2015) and Abera et al. (2020), who led toward the existence of severe hydroclimatic gradients along the highland-lowland zone.

Compared to benchmark indices such as NDVI, VCI, and SPEI, the SAED-ViT model exhibited better alignment with validated drought development timelines. As demonstrated in Figure 14, traditional indices tended to lag or excessively smooth multi-season drought events, while SAED-ViT consistently captured both onset and recovery phases. This sensitivity is brought about by the design of the MAE-ViT model to retain high-order interactions between seasonal NDVI, LST, and precipitation signals—previously recognized factors as being synergistic in identifying drought (Afshar et al., 2021; Duan et al., 2025).

Furthermore, proxy validation against SPEI (Figures 12 and 13) confirms the robustness of SAED-ViT. The inverse relationship between the frequency of extreme drought regimes and SPEI values reinforces the model's semantic alignment with hydrological stress. This consistency is significant as SPEI has been extensively used as one of the most reliable indicators of severity of drought in a diversity of climates (J. Dong et al., 2023; Vicente-Serrano et al., 2010). Our finding agrees with Mehravar et al. (2021), who emphasized the quality of blending thermal and vegetative indices to improve correlation with SPEI-based assessment.

Though SPEI was employed as our primary validation reference, our research was not limited to a single index. SAED-ViT performance was further compared with vegetation- and temperature-based indices like NDVI, VCI, and VHI, which are well-established measures of crop stress and droughts. Outcomes showed that SAED-ViT consistently outperformed the indices, particularly in identifying the beginning and end of droughts and thereby affirming its robustness over multiple proxy variables. Given these outcomes, cross-validation against additional data such as soil moisture (e.g., SMAP, ESA CCI), crop yield anomaly, or socioeconomic drought impact indices would likely produce minimal differences in performance and would not alter overall conclusions. This supposition agrees with previous studies across East Africa indicating that SPEI, vegetation indexes, and soil moisture data sets correlate highly in delineating drought mechanisms (Alasow et al., 2024; Epule et al., 2024; Mehravar et al., 2021).

From a machine learning perspective, the self-supervised nature of the MAE-ViT encoder introduces a crucial advantage for drought monitoring in data-scarce regions. Previous models used to employ supervised learning, and that demanded ground-truth labels that are hardly present or reliable within the HOA (Cortés-Andrés et al., 2024; Gyaneshwar et al., 2023). Conversely, the SAED-ViT model circumvents such a bottleneck by reconstructing missing spatial patches and extracting latent drought representations directly from input anomalies, a strategy recently advocated by Fan et al. (2025); and He et al. (2022) in other domains of remote sensing.

Cluster-based drought classification is also a methodological novelty. Unlike traditional drought classes defined by hard thresholds, our model uses latent features to induce empirically significant regimes. Intra-cluster variability analysis (Figure 5) reveals that clusters not only differ in mean anomaly values but also in their internal heterogeneity, an aspect seldom incorporated in existing drought frameworks. This aligns with the recommendations of Ghazaryan et al. (2020); and Hao and Singh (2015), who encouraged multi-dimensional and variance-aware drought definitions.

Validation of silhouette and Calinski-Harabasz cluster validity indices (Section 2.3.3) confirms structural homogeneity within the unsupervised drought classes. Our silhouette value (∼0.59) is positively comparable to recent environmental classification benchmarks (Januzaj et al., 2023; Lukasik et al., 2016), indicating well-separated and densely packed clusters. This statistical robustness also adds credibility to empirical semantic cluster labeling (e.g., Extreme, Mild, Normal).

Interestingly, the SAED-ViT map spatial patterns are also consistent with regional hydrological and agricultural conditions. The persistent classification of southeastern Ethiopia and southern Somalia as "Severe" or "Extreme" is supported by historical crop failure events and food security crises (Epule et al., 2024; Warsame et al., 2021). Contrarily, western Ethiopia and Eritrea stability in OND is consistent with orographic rainfall-increasing features and increased vegetation cover documented by Abera et al. (2020); and Joordens et al. (2019). The visual coherence and ecological realism of such outputs validate the model to detect region-specific drought dynamics at different spatial scales.

Although this study focuses on the Horn of Africa, the SAED-ViT architecture is applicable to any other dry regions. With only remotely sensed global data such as MODIS NDVI, MODIS LST, and CHIRPS precipitation, the model is location-independent for calibrations and labeled drought records. Its deviation-based embedding strategy learns departure patterns relative to local climatological baselines rather than absolute values, therefore enhancing its ability to generalize across ecosystems with disparate agro-climatic regimes. Initial experiments across Kenya and Sudan confirmed that SAED-ViT had consistent clustering features and powerful anomaly detection outside the Horn of Africa, in line with new studies indicating self-supervised anomaly based models have the ability to generalize effectively within diverse environments (Cortés-Andrés et al., 2024; Qin et al., 2021). Furthermore, the application of globally harmonized inputs enhances the potential of the model to be implemented in South Asia and South America (Duan et al., 2025), where sparsity of observational data hits drought monitoring as well but where exposure to agricultural drought is critically high (Ma et al., 2019; Xue et al., 2025). Future work will systematically validate the scalability of SAED-ViT across these regions by incorporating local agricultural and socioeconomic drought impact data with satellite-guided anomaly embeddings to assess cross-regional performance.

Despite its strengths, the SAED-ViT system does present certain limitations. Although effective for detecting meso-scale variability, the use of 4×4 spatial patches may compromise hyperlocal dynamics, particularly in regions with heterogeneous land use. And while the model indirectly cross-validates effectively against SPEI, the direct yield or socioeconomic impacts were not modeled due to a lack of ground truth. In future work, we aim to enhance the SAED-ViT framework by incorporating soil moisture and evapotranspiration products to capture additional hydrometeorological dimensions of drought. These variables can improve the model's responsiveness to both agricultural and hydrological drought, especially in regions where vegetation or temperature anomalies alone may not fully represent water stress.

Even with its advantages, the SAED-ViT architecture is limited by its use of fixed spatial patch sizes that potentially discount localized drought subtleties and by the absence of socioeconomic impact integration. The inclusion of crop yield observations, soil moisture levels, and socio-environmental factors in future work would improve interpretability and operationality. Adaptive patching and multi-scale architectures could also further tailor spatial sensitivity to complex landscapes.

5. Conclusion

Drought remains one of the most pressing climate-related hazards in the Horn of Africa, with significant impacts on agriculture, food security, and livelihoods, exacerbated by a lack of ground-based monitoring networks. To address this gap, we proposed SAED-ViT—a novel, label-free drought monitoring framework that integrates seasonal anomaly embeddings of NDVI, LST, and rainfall with self-supervised feature learning using masked autoencoders and Vision Transformers. This strategy enables the model to learn latent drought-relevant representations in time and space without labeled data sets, the primary innovation for data-poor environments. Unsupervised K-Means clustering of the learned features allowed the emergence of empirically interpretable drought regimes, which were mapped into severity classes and tracked for 25 years.

In terms of both visual and statistical consistency, the SAED-ViT system surpassed traditional indices like NDVI anomalies, TCI, and VHI. It also demonstrated strong temporal and spatial consistency with the SPEI ($r = -0.909$ P-value < 0.01). The model successfully replicated long-term drought patterns and seasonal variations, identifying well-documented drought years (e.g., 2011, 2017, and 2022) and capturing spatial transitions often missed by conventional univariate approaches.

This work demonstrates that deep self-supervised models hold the potential to resolve one of the methodological bottlenecks in drought monitoring through enabling scalable, explainable, and context-aware classification. The SAED-ViT system lays the groundwork for future real-time, global drought alert systems that require no labeled data and are equipped to handle the growing complexity of climate-related hazards.

Conflict of Interest

The authors declare that they have no known competing financial interests or personal relationships that could have appeared to influence the work reported in this paper.

Data Availability Statement

The MODIS Terra NDVI (MOD13Q1) and LST (MOD11A2) data sets were obtained from NASA LP DAAC (Didan, 2015; Wan et al., 2015). Precipitation data were retrieved from the CHIRPS data set (Funk et al., 2015). Potential evapotranspiration was derived from ERA5-Land monthly reanalysis (Muñoz Sabater, 2019a, 2019b). The Standardized Precipitation Evapotranspiration Index (SPEI) used for validation was calculated using the SPEI *R* package (Beguería et al., 2014). All model implementation code, including preprocessing, anomaly stacking, MAE-ViT self-supervised training, clustering, and drought classification pipeline, is archived on Zenodo (nasserah, 2025).

References

Abdelrahim, N. A. M., & Jin, S. (2025a). A novel Agricultural Remote Sensing Drought Index (ARSDI) for high-resolution drought assessment in Africa using Sentinel and Landsat data. *Environmental Monitoring and Assessment*, *197*(3), 242. https://doi.org/10.1007/s10661-025-13686-3

Abdelrahim, N. A. M., & Jin, S. (2025b). Continental maize mapping and distribution in Africa by integrating radar and optical imagery. *Environmental Monitoring and Assessment*, *197*(9), 1072. https://doi.org/10.1007/s10661-025-14502-8

Abdelrahim, N. A. M., & Jin, S. (2025c). Genetic Algorithm Optimized Multispectral Soil-Vegetation Drought Index (GA-MSVDI) for precision agriculture and drought monitoring in North Africa. *Remote Sensing Applications: Society and Environment*, *38*, 101603. https://doi.org/10.1016/j.rsase.2025.101603

Abebe, B. W., Mana, T. T., & Hatiye, S. D. (2024). Assessment of meteorological drought and its association with global climate drivers in Genale Dawa river basin, South-East of Ethiopia. *Modeling Earth Systems and Environment*, *10*(4), 5027–5042. https://doi.org/10.1007/s40808-024-02048-6

Abera, T. A., Heiskanen, J., Pellikka, P. K. E., & Maeda, E. E. (2020). Impact of rainfall extremes on energy exchange and surface temperature anomalies across biomes in The Horn Of Africa. *Agricultural and Forest Meteorology*, *280*, 107779. https://doi.org/10.1016/j.agrformet.2019.107779

Adhikari, S., Zhou, W., Dou, Z., Sakib, N., Ma, R., Chaudhari, B., & Liu, B. (2024). Analysis of Flash drought and its impact on forest Normalized Difference Vegetation Index (NDVI) in Northeast China from 2000 to 2020. *Atmosphere*, *15*(7), 818. https://doi.org/10.3390/atmos15070818

Adloff, M., Singer, M. B., MacLeod, D. A., Michaelides, K., Mehrnegar, N., Hansford, E., et al. (2022). Sustained water storage in Horn of Africa drylands dominated by seasonal rainfall extremes. *Geophysical Research Letters*, *49*(21), e2022GL099299. https://doi.org/10.1029/2022GL099299

Afshar, M. H., Al-Yaari, A., & Yilmaz, M. T. (2021). Comparative evaluation of microwave L-Band VOD and optical NDVI for agriculture drought detection over central Europe. *Remote Sensing*, *13*(7), 1251. https://doi.org/10.3390/rs13071251

Afuecheta, E., & Omar, M. H. (2021). Characterization of variability and trends in daily precipitation and temperature extremes in The Horn of Africa. *Climate Risk Management*, *32*, 100295. https://doi.org/10.1016/j.crm.2021.100295

Agarwal, V., Bhanwar, S., Stuart, M., Zhengyuan, Q., Sen, A., & Kulhari, K. (2025). Integrated remote sensing for enhanced drought assessment: A multi-index approach in Rajasthan, India. *Earth and Space Science*, *12*(2), e2024EA003639. https://doi.org/10.1029/2024EA003639

AghaKouchak, A. (2015). A multivariate approach for persistence-based drought prediction: Application to the 2010–2011 East Africa drought. *Journal of Hydrology*, *526*, 127–135. https://doi.org/10.1016/j.jhydrol.2014.09.063

Agutu, N. O., Awange, J. L., Ndehedehe, C., & Mwaniki, M. (2020). Consistency of agricultural drought characterization over upper greater Horn Of Africa (1982–2013): Topographical, gauge density, and model forcing influence. *Science of the Total Environment*, *709*, 135149. https://doi.org/10.1016/j.scitotenv.2019.135149

Ahmadi, H., Mahdimahalleh, S. E., Farahat, A., & Saffari, B. (2025). Unsupervised time-series signal analysis with autoencoders and vision transformers: A review of architectures and applications. *Journal of Intelligent Learning Systems and Applications*, *17*(2), 77–111. https://doi.org/10.4236/jilsa.2025.172007

Alahacoon, N., Edirisinghe, M., & Ranagalage, M. (2021). Satellite-based meteorological and agricultural drought monitoring for agricultural sustainability in Sri Lanka. *Sustainability*, *13*(6), 3427. https://doi.org/10.3390/su13063427

Alasow, A. A., Hamed, M. M., & Shahid, S. (2024). Spatiotemporal variability of drought and affected croplands in The Horn Of Africa. *Stochastic Environmental Research and Risk Assessment*, *38*(1), 281–296. https://doi.org/10.1007/s00477-023-02575-1

Alexander, C. (2020). Normalised difference spectral indices and urban land cover as indicators of Land Surface Temperature (LST). *International Journal of Applied Earth Observation and Geoinformation*, *86*, 102013. https://doi.org/10.1016/j.jag.2019.102013

Alito, K. T., & Kerebih, M. S. (2024). Spatio-temporal assessment of agricultural drought using remote sensing and ground-based data indices in the Northern Ethiopian highland. *Journal of Hydrology: Regional Studies*, *52*, 101700. https://doi.org/10.1016/j.ejrh.2024.101700

Al-Kilani, M. R., Al-Bakri, J., Rahbeh, M., Abdelal, Q., Yalew, S., & Mul, M. (2024). Assessment of meteorological drought impacts on rainfed agriculture using remote sensing–derived biomass productivity. *Environmental Monitoring and Assessment*, *196*(10), 879. https://doi.org/10.1007/s10661-024-13061-8

Al-Quraishi, A. M. F., Gaznayee, H. A., & Crespi, M. (2021). Drought trend analysis in a semi-arid area of Iraq based on normalized difference vegetation index, normalized difference water index and standardized precipitation index. *Journal of Arid Land*, *13*(4), 413–430. https://doi.org/10.1007/s40333-021-0062-9

Bedasa, Y., & Bedemo, A. (2022). The effect of climate change on food insecurity in The Horn of Africa. *Geojournal*, *88*(2), 1829–1839. https://doi.org/10.1007/s10708-022-10733-1

Beguería, S., Vicente-Serrano, S. M., Reig, F., & Latorre, B. (2014). Standardized Precipitation Evapotranspiration Index (SPEI) revisited: Parameter fitting, evapotranspiration models, tools, datasets and drought monitoring. *International Journal of Climatology*, *34*(10), 3001–3023. https://doi.org/10.1002/joc.3887

Bento, V. A., Gouveia, C. M., DaCamara, C. C., Libonati, R., & Trigo, I. F. (2020). The roles of NDVI and land surface temperature when using the vegetation health index over dry regions. *Global and Planetary Change*, *190*, 103198. https://doi.org/10.1016/j.gloplacha.2020.103198

Beyene, T. K., Agarwal, A., Jain, M. K., & Yadav, B. K. (2023). Investigation of the propagation of meteorological to hydrological drought and water required to recover from drought over Ethiopian basins. *Journal of Water and Climate Change*, *14*(9), 2988–3009. https://doi.org/10.2166/wcc.2023.024

Bhardwaj, K., Shah, D., Aadhar, S., & Mishra, V. (2020). Propagation of meteorological to hydrological droughts in India. *Journal of Geophysical Research: Atmospheres*, *125*(22), e2020JD033455. https://doi.org/10.1029/2020JD033455

Bora, A., Calklins, J., & Joykutty, L. (2024). Creating a drought prediction model using convolutional neural networks. *Journal of Emerging Investigators*. https://doi.org/10.59720/23-094

Brandt, M., Hiernaux, P., Rasmussen, K., Mbow, C., Kergoat, L., Tagesson, T., et al. (2016). Assessing woody vegetation trends in Sahelian drylands using MODIS based seasonal metrics. *Remote Sensing of Environment*, *183*, 215–225. https://doi.org/10.1016/j.rse.2016.05.027

Cao, M., Chen, M., Liu, J., & Liu, Y. (2022). Assessing the performance of satellite soil moisture on agricultural drought monitoring in the North China plain. *Agricultural Water Management*, *263*, 107450. https://doi.org/10.1016/j.agwat.2021.107450

Cortés-Andrés, J., Fernández-Torres, M.-Á., & Camps-Valls, G. (2024). Deep learning with noisy Labels for spatiotemporal drought detection. *IEEE Transactions on Geoscience and Remote Sensing*, *62*, 1–13. https://doi.org/10.1109/TGRS.2024.3504340

D'Ercole, R., Casella, D., Panegrossi, G., & Sanò, P. (2024). A high temporal resolution NDVI time series to monitor drought events in The Horn Of Africa. *International Journal of Applied Earth Observation and Geoinformation*, *135*, 104264. https://doi.org/10.1016/j.jag.2024.104264

Didan, K. (2015). MOD13Q1 MODIS/Terra vegetation indices 16-day L3 global 250 m SIN grid V006 [Dataset]. *NASA EOSDIS Land Processes DAAC*. https://doi.org/10.5067/MODIS/MOD13Q1.006

Dinku, T., Funk, C., Peterson, P., Maidment, R., Tadesse, T., Gadain, H., & Ceccato, P. (2018). Validation of the CHIRPS satellite rainfall estimates over eastern Africa. *Quarterly Journal of the Royal Meteorological Society*, *144*(S1), 292–312. https://doi.org/10.1002/qj.3244

Dong, J., Xing, L., Cui, N., Zhao, L., Guo, L., & Gong, D. (2023). Standardized Precipitation Evapotranspiration Index (SPEI) estimated using variant long short-term memory network at four climatic zones of China. *Computers and Electronics in Agriculture*, *213*, 108253. https://doi.org/10.1016/j.compag.2023.108253

Dong, Z., & Jin, S. G. (2021). Evaluation of the land GNSS-reflected DDM coherence on soil moisture estimation from CYGNSS data. *Remote Sensing*, *13*(4), 570. https://doi.org/10.3390/rs13040570

Du, L., Tian, Q., Yu, T., Meng, Q., Jancso, T., Udvardy, P., & Huang, Y. (2013). A comprehensive drought monitoring method integrating MODIS and TRMM data. *International Journal of Applied Earth Observation and Geoinformation*, *23*, 245–253. https://doi.org/10.1016/j.jag.2012.09.010

Duan, X., Aslam, R. W., Naqvi, S. A. A., Kucher, D. E., Afzal, Z., Raza, D., et al. (2025). Multi-index assessment and machine learning integration for drought monitoring in Yunnan, China, using google Earth engine. *Ieee Journal of Selected Topics in Applied Earth Observations and Remote Sensing*, 1–23. https://doi.org/10.1109/JSTARS.2025.3580652

Edokossi, K., Calabia, A., Jin, S., & Molina, I. (2020). GNSS-reflectometry and remote sensing of soil moisture: A review of measurement techniques, methods, and applications. *Remote Sensing*, *12*(4), 614. https://doi.org/10.3390/rs12040614

Edokossi, K., Jin, S., Calabia, A., Molina, I., & Mazhar, U. (2024). Evaluation of SMAP and CYGNSS soil moistures in drought prediction using multiple linear regression and GLDAS product. *Photogrammetric Engineering & Remote Sensing*, *90*(5), 303–312. https://doi.org/10.14358/pers.23-00075r2

Epule, T. E., Chehbouni, A., Dhiba, D., & Molua, E. L. (2024). A regional stocktake of maize yield vulnerability to droughts in The Horn Of Africa. *Environmental Monitoring and Assessment*, *196*(1), 76. https://doi.org/10.1007/s10661-023-12229-y

Ezzahra, F. F., Ahmed, A., & Abdellah, A. (2023). Variance-based fusion of VCI and TCI for efficient classification of agriculture drought using Landsat data in the high atlas (Morocco, North Africa). *Nature Environment and Pollution Technology*, *22*(3), 1421–1429. https://doi.org/10.46488/NEPT.2023.v22i03.028

Fan, H., Cheng, S., De Nazelle, A. J., & Arcucci, R. (2025). ViTAE-SL: A vision transformer-based autoencoder and spatial interpolation learner for field reconstruction. *Computer Physics Communications*, *308*, 109464. https://doi.org/10.1016/j.cpc.2024.109464

FAO, F. (2019). *The state of food security and nutrition in the world 2019: Safeguarding against economic slowdowns and downturns* (1st ed.). United Nations Publications.

Farrag, A., Mostafa, G., & Mohamed, A. (2020). Detecting land cover changes using VHR satellite images: A comparative study. *JES. Journal of Engineering Sciences*, *48*(No 2), 200–211. https://doi.org/10.21608/jesaun.2019.264927

Funk, C., Peterson, P., Landsfeld, M., Pedreros, D., Verdin, J., Shukla, S., et al. (2015). Climate Hazards Group InfraRed Precipitation with Station data (CHIRPS) [Dataset]. *UC Santa Barbara Climate Hazards Center*. https://doi.org/10.15780/G2RP4Q

Ghazaryan, G., Dubovyk, O., Graw, V., Kussul, N., & Schellberg, J. (2020). Local-scale agricultural drought monitoring with satellite-based multi-sensor time-series. *GIScience and Remote Sensing*, *57*(5), 704–718. https://doi.org/10.1080/15481603.2020.1778332

Gyaneshwar, A., Mishra, A., Chadha, U., Raj Vincent, P. M. D., Rajinikanth, V., Pattukandan Ganapathy, G., & Srinivasan, K. (2023). A contemporary review on deep learning models for drought prediction. *Sustainability*, *15*(7), 6160. https://doi.org/10.3390/su15076160

Ha, T. V., Uereyen, S., & Kuenzer, C. (2023). Agricultural drought conditions over mainland Southeast Asia: Spatiotemporal characteristics revealed from MODIS-based vegetation time-series. *International Journal of Applied Earth Observation and Geoinformation*, *121*, 103378. https://doi.org/10.1016/j.jag.2023.103378

Habte, A., Worku, W., Mamo, G., Ayalew, D., & Gayler, S. (2023). Rainfall variability and its seasonal events with associated risks for rainfed crop production in Southwest Ethiopia. *Cogent Food & Agriculture*, *9*(1), 2231693. https://doi.org/10.1080/23311932.2023.2231693

Han, X., Li, Y., Yu, W., & Feng, L. (2022). Attribution of the extreme drought in The Horn Of Africa during short-rains of 2016 and long-rains of 2017. *Water*, *14*(3), 409. https://doi.org/10.3390/w14030409

Hao, Z., Hao, F., Xia, Y., Feng, S., Sun, C., Zhang, X., et al. (2022). Compound droughts and hot extremes: Characteristics, drivers, changes, and impacts. *Earth-Science Reviews*, *235*, 104241. https://doi.org/10.1016/j.earscirev.2022.104241

Hao, Z., & Singh, V. P. (2015). Drought characterization from a multivariate perspective: A review. *Journal of Hydrology*, *527*, 668–678. https://doi.org/10.1016/j.jhydrol.2015.05.031

He, K., Chen, X., Xie, S., Li, Y., Dollar, P., & Girshick, R. (2022). Masked autoencoders are scalable vision learners. In *2022 IEEE/CVF Conference on Computer Vision and Pattern Recognition (CVPR)* (pp. 15979–15988). https://doi.org/10.1109/CVPR52688.2022.01553

Isinkaye, F. O., Olusanya, M. O., & Akinyelu, A. A. (2025). A multi-class hybrid variational autoencoder and vision transformer model for enhanced plant disease identification. *Intelligent Systems with Applications*, *26*, 200490. https://doi.org/10.1016/j.iswa.2025.200490

Jalayer, S., Sharifi, A., Abbasi-Moghadam, D., Tariq, A., & Qin, S. (2023). Assessment of spatiotemporal characteristic of droughts using in situ and remote sensing-based drought indices. *IEEE Journal of Selected Topics in Applied Earth Observations and Remote Sensing*, *16*, 1483–1502. https://doi.org/10.1109/JSTARS.2023.3237380

Januzaj, Y., Beqiri, E., & Luma, A. (2023). Determining the optimal number of clusters using silhouette score as a data mining technique. *International Journal of Online and Biomedical Engineering (iJOE)*, *19*(4), 174–182. https://doi.org/10.3991/ijoe.v19i04.37059

Jiang, L., Gao, W., Zhu, K., Zheng, J., & Ren, B. (2025). Why did the extreme drought in the Yangtze River basin in 2022 break the 2019 record? *Earth and Space Science*, *12*(3), e2024EA003972. https://doi.org/10.1029/2024EA003972

Jiao, W., Zhang, L., Chang, Q., Fu, D., Cen, Y., & Tong, Q. (2016). Evaluating an enhanced Vegetation Condition Index (VCI) based on VIUPD for drought monitoring in the Continental United States. *Remote Sensing*, *8*(3), 224. https://doi.org/10.3390/rs8030224

Jin, S., Camps, A., Jia, Y., Wang, F., Martin-Neira, M., Huang, F., et al. (2024). Remote sensing and its applications using GNSS reflected signals: Advances and prospects. *Satellite Navigation*, *5*(1), 19. https://doi.org/10.1186/s43020-024-00139-4

Jin, S., Chen, Z., & Peng, H. (2025). High-frequency centimeter-accuracy water level estimation in the Yangtze River using Multi-GNSS interferometric reflectometry. *IEEE Transactions on Geoscience and Remote Sensing*, *63*, 5802713. https://doi.org/10.1109/tgrs.2025.3594071

Joordens, J. C. A., Feibel, C. S., Vonhof, H. B., Schulp, A. S., & Kroon, D. (2019). Relevance of the eastern African coastal forest for early hominin biogeography. *Journal of Human Evolution*, *131*, 176–202. https://doi.org/10.1016/j.jhevol.2019.03.012

Jury, M. R. (2023). Characterizing Northeast Africa drought and its drivers. *Climate*, *11*(6), 130. https://doi.org/10.3390/cli11060130

Kalisa, W., Zhang, J., Igbawua, T., Ujoh, F., Ebohon, O. J., Namugize, J. N., & Yao, F. (2020). Spatio-temporal analysis of drought and return periods over the East African region using standardized precipitation index from 1920 to 2016. *Agricultural Water Management*, *237*, 106195. https://doi.org/10.1016/j.agwat.2020.106195

Kan, J.-C., Ferreira, C. S. S., Destouni, G., Haozhi, P., Vieira Passos, M., Barquet, K., & Kalantari, Z. (2023). Predicting agricultural drought indicators: ML approaches across wide-ranging climate and land use conditions. *Ecological Indicators*, *154*, 110524. https://doi.org/10.1016/j.ecolind.2023.110524

Khorrami, B., & Gündüz, O. (2022). Detection and analysis of drought over Turkey with remote sensing and model-based drought indices. *Geocarto International*, *37*(26), 12171–12193. https://doi.org/10.1080/10106049.2022.2066197

Khorrami, B., Sahin, O. G., & Gunduz, O. (2024). Comprehensive comparison of different gridded precipitation products over geographic regions of Türkiye. *Journal of Applied Remote Sensing*, *18*(3). https://doi.org/10.1117/1.JRS.18.034503

Kogan, F. N. (1997). Global drought watch from space. *Bulletin of the American Meteorological Society*, *78*(4), 621–636. https://doi.org/10.1175/1520-0477(1997)078<0621:GDWFS>2.0.CO;2

Kourouma, J. M., Eze, E., Kelem, G., Negash, E., Phiri, D., Vinya, R., et al. (2022). Spatiotemporal climate variability and meteorological drought characterization in Ethiopia. *Geomatics, Natural Hazards and Risk*, *13*(1), 2049–2085. https://doi.org/10.1080/19475705.2022.2106159

Kumar, D., Soni, A., & Kumar, M. (2022). Retrieval of land surface temperature from Landsat-8 thermal infrared Sensor data. *Journal of Human, Earth, and Future*, *3*(2), 159–168. https://doi.org/10.28991/HEF-2022-03-02-02

Leal Filho, W., Djekic, I., Smetana, S., & Kovaleva, M. (Eds.) (2022). *Handbook of climate change across the food supply chain*. Springer International Publishing. https://doi.org/10.1007/978-3-030-87934-1

Li, B., Liang, S., Ma, H., Dong, G., Liu, X., He, T., & Zhang, Y. (2024). Generation of global 1 km all-weather instantaneous and daily mean land surface temperatures from MODIS data. *Earth System Science Data*, *16*(8), 3795–3819. https://doi.org/10.5194/essd-16-3795-2024

Li, Y., Huang, S., Wang, H., Zheng, X., Huang, Q., Deng, M., & Peng, J. (2022). High-resolution propagation time from meteorological to agricultural drought at multiple levels and spatiotemporal scales. *Agricultural Water Management*, *262*, 107428. https://doi.org/10.1016/j.agwat.2021.107428

Liu, J., Huang, X., Zheng, J., Liu, Y., & Li, H. (2023). MixMAE: Mixed and masked autoencoder for efficient pretraining of hierarchical vision transformers. In *2023 IEEE/CVF Conference on Computer Vision and Pattern Recognition (CVPR)* (pp. 6252–6261). https://doi.org/10.1109/CVPR52729.2023.00605

Lukasik, S., Kowalski, P. A., Charytanowicz, M., & Kulczycki, P. (2016). Clustering using flower pollination algorithm and Calinski-Harabasz index. In *2016 IEEE Congress on Evolutionary Computation (CEC)* (pp. 2724–2728). https://doi.org/10.1109/cec.2016.7744132

Lyon, B. (2014). Seasonal drought in the greater Horn Of Africa and its recent increase during the March–May long rains. *Journal of Climate*, *27*(21), 7953–7975. https://doi.org/10.1175/JCLI-D-13-00459.1

Ma, L., Liu, Y., Zhang, X., Ye, Y., Yin, G., & Johnson, B. A. (2019). Deep learning in remote sensing applications: A meta-analysis and review. *ISPRS Journal of Photogrammetry and Remote Sensing*, *152*, 166–177. https://doi.org/10.1016/j.isprsjprs.2019.04.015

Mall, U., Phoo, C. P., Liu, M. K., Vondrick, C., Hariharan, B., & Bala, K. (2023). Remote sensing vision-language foundation models without annotations via ground remote alignment (arXiv:2312.06960). *arXiv*. https://doi.org/10.48550/arXiv.2312.06960

Mao, Z., Tong, X., Luo, Z., & Zhang, H. (2022). MFATNet: Multi-scale feature aggregation via transformer for remote sensing image change detection. *Remote Sensing*, *14*(21), 5379. https://doi.org/10.3390/rs14215379

Masroor, M., Sajjad, H., Rehman, S., Singh, R., Hibjur Rahaman, M., Sahana, M., et al. (2022). Analysing the relationship between drought and soil erosion using vegetation health index and Rusle models in Godavari middle sub-basin, India. *Geoscience Frontiers*, *13*(2), 101312. https://doi.org/10.1016/j.gsf.2021.101312

Mbatha, N., & Xulu, S. (2018). Time series analysis of MODIS-derived NDVI for the Hluhluwe-Imfolozi Park, South Africa: Impact of recent intense drought. *Climate*, *6*(4), 95. https://doi.org/10.3390/cli6040095

Measho, S., Chen, B., Pellikka, P., Trisurat, Y., Guo, L., Sun, S., & Zhang, H. (2020). Land use/land cover changes and associated impacts on water yield availability and variations in the Mereb-gash river basin in The Horn Of Africa. *Journal of Geophysical Research: Biogeosciences*, *125*(7), e2020JG005632. https://doi.org/10.1029/2020JG005632

Mehravar, S., Amani, M., Moghimi, A., Dadrass Javan, F., Samadzadegan, F., Ghorbanian, A., et al. (2021). Temperature-Vegetation-soil Moisture-Precipitation Drought Index (TVMPDI); 21-year drought monitoring in Iran using satellite imagery within google Earth engine. *Advances in Space Research*, *68*(11), 4573–4593. https://doi.org/10.1016/j.asr.2021.08.041

Mei, S., Lian, J., Wang, X., Su, Y., Ma, M., & Chau, L.-P. (2024). A comprehensive study on the robustness of deep learning-based image classification and object detection in remote sensing: Surveying and benchmarking. *Journal of Remote Sensing*, *4*, 0219. https://doi.org/10.34133/remotesensing.0219

Moghimi, M. M., & Zarei, A. R. (2021). Evaluating performance and applicability of several drought indices in arid regions. *Asia-Pacific Journal of Atmospheric Sciences*, *57*(3), 645–661. https://doi.org/10.1007/s13143-019-00122-z

Mostafa, Y., Mohamed, N., & Farrag, A. F. (2021). Change detection for map updating using ◆very high resolution satellite images. *JES. Journal of Engineering Sciences*, 424–445. https://doi.org/10.21608/jesaun.2021.67949.1039

Muñoz Sabater, J. (2019a). ERA5-Land monthly averaged data from 1981 to present [Dataset]. *Copernicus Climate Change Service (C3S) Climate Data Store*. https://doi.org/10.24381/cds.68d2bb30

Muñoz Sabater, J. (2019b). ERA5-Land monthly averaged data from 1950 to present [Dataset]. *Copernicus Climate Data Store*. Retrieved from https://cds.climate.copernicus.eu/datasets/reanalysis-era5-land-monthly-means?tab=download

Najibi, N., & Jin, S. (2013). Physical reflectivity and polarization characteristics for snow and ice-covered surfaces interacting with GPS signals. *Remote Sensing*, *5*(8), 4006–4030. https://doi.org/10.3390/rs5084006

nasserah. (2025). nasserah/SAED-ViT: Saed-vit (version 1.0) [Software]. *Zenodo*. https://doi.org/10.5281/zenodo.16320221

Naumann, G., Barbosa, P., Garrote, L., Iglesias, A., & Vogt, J. (2014). Exploring drought vulnerability in Africa: An indicator based analysis to be used in early warning systems. *Hydrology and Earth System Sciences*, *18*(5), 1591–1604. https://doi.org/10.5194/hess-18-1591-2014

Nguyen, H., Wheeler, M. C., Otkin, J. A., Nguyen-Huy, T., & Cowan, T. (2023). Climatology and composite evolution of flash drought over Australia and its vegetation impacts. *Journal of Hydrometeorology*, *24*(6), 1087–1101. https://doi.org/10.1175/JHM-D-22-0033.1

Nicholson, S. E. (2014). The predictability of rainfall over the greater Horn Of Africa. Part I: Prediction of seasonal rainfall. *Journal of Hydrometeorology*, *15*(3), 1011–1027. https://doi.org/10.1175/JHM-D-13-062.1

Niu, Y., Song, Z., Luo, Q., Chen, G., Ma, M., & Li, F. (2025). ATMformer: An adaptive token merging vision transformer for remote sensing image scene classification. *Remote Sensing*, *17*(4), 660. https://doi.org/10.3390/rs17040660

Olawade, D. B., Wada, O. Z., Ige, A. O., Egbewole, B. I., Olojo, A., & Oladapo, B. I. (2024). Artificial intelligence in environmental monitoring: Advancements, challenges, and future directions. *Hygiene and Environmental Health Advances*, *12*, 100114. https://doi.org/10.1016/j.heha.2024.100114

Omar, A. O., Alasow, A. A., Farah, A. A., & Shahid, S. (2024). Spatiotemporal analysis of agricultural drought severity and hotspots in Somaliland. *International Journal of Sustainable Development and Planning*, *19*(11), 4135–4146. https://doi.org/10.18280/ijsdp.191104

Ornella, L., Kruseman, G., & Crossa, J. (2020). Satellite data and supervised learning to prevent impact of drought on crop production: Meteorological drought. In G. Ondrasek (Ed.), *Drought—detection and solutions*. IntechOpen. https://doi.org/10.5772/intechopen.85471

Prodhan, F. A., Zhang, J., Hasan, S. S., Pangali Sharma, T. P., & Mohana, H. P. (2022). A review of machine learning methods for drought hazard monitoring and forecasting: Current research trends, challenges, and future research directions. *Environmental Modelling & Software*, *149*, 105327. https://doi.org/10.1016/j.envsoft.2022.105327

Qin, Q., Wu, Z., Zhang, T., Sagan, V., Zhang, Z., Zhang, Y., et al. (2021). Optical and thermal remote sensing for monitoring agricultural drought. *Remote Sensing*, *13*(24), 5092. https://doi.org/10.3390/rs13245092

Rajeshwari, A., & Mani, N. D. (2014). Estimation of land surface temperature of dindigul district using Landsat 8 data. *International Journal of Renewable Energy Technology*, *3*(5), 122–126. https://doi.org/10.15623/ijret.2014.0305025

Rajsekhar, D., Singh, V. P., & Mishra, A. K. (2015). Multivariate drought index: An information theory based approach for integrated drought assessment. *Journal of Hydrology*, *526*, 164–182. https://doi.org/10.1016/j.jhydrol.2014.11.031

Raza, M. O., Mahoto, N. A., Al Reshan, M. S., Alqazzaz, A., Rajab, A., & Shaikh, A. (2025). Drought detection in satellite imagery: A layered ensemble machine learning approach. *International Journal of Computational Intelligence Systems*, *18*(1), 161. https://doi.org/10.1007/s44196-025-00903-7

Rincón-Avalos, P., Khouakhi, A., Mendoza-Cano, O., & Paredes-Bonilla, K. M. (2022). Evaluation of satellite precipitation products over Mexico using Google Earth Engine. https://doi.org/10.2166/hydro.2022.122

Sadam Hussain Hingoro, S. A. (2025). Integrating remote sensing and deep learning for agricultural drought monitoring. https://doi.org/10.5281/ZENODO.15662336

Sajid, M., Razzaq Malik, K., Ur Rehman, A., Safdar Malik, T., Alajmi, M., Haider Khan, A., et al. (2025). Leveraging two-dimensional pretrained vision transformers for three-dimensional model generation via masked autoencoders. *Scientific Reports*, *15*(1), 3164. https://doi.org/10.1038/s41598-025-87376-y

Scheuerer, M., Bahaga, T. K., Segele, Z. T., & Thorarinsdottir, T. L. (2024). Probabilistic rainy season onset prediction over the greater Horn Of Africa based on long-range multi-model ensemble forecasts. *Climate Dynamics*, *62*(5), 3587–3604. https://doi.org/10.1007/s00382-023-07085-y

Shahapure, K. R., & Nicholas, C. (2020). Cluster quality analysis using silhouette score. In *2020 IEEE 7th International Conference on data Science and Advanced Analytics (DSAA)* (pp. 747–748). https://doi.org/10.1109/dsaa49011.2020.00096

Shen, Z., Zhang, Q., Singh, V. P., Sun, P., Song, C., & Yu, H. (2019). Agricultural drought monitoring across Inner Mongolia, China: Model development, spatiotemporal patterns and impacts. *Journal of Hydrology*, *571*, 793–804. https://doi.org/10.1016/j.jhydrol.2019.02.028

Shikhar, S., & Sobti, A. (2024). Label-free anomaly detection in aerial agricultural images with masked image modeling. In *2024 IEEE/CVF Conference on Computer Vision and Pattern Recognition Workshops (CVPRW)* (pp. 5440–5449). https://doi.org/10.1109/cvprw63382.2024.00553

Sobrino, J. A., Oltra-Carrió, R., Sòria, G., Jiménez-Muñoz, J. C., Franch, B., Hidalgo, V., et al. (2013). Evaluation of the surface urban heat island effect in the city of Madrid by thermal remote sensing. *International Journal of Remote Sensing*, *34*(9–10), 3177–3192. https://doi.org/10.1080/01431161.2012.716548

Tierney, J. E., Ummenhofer, C. C., & de Menocal, P. B. (2015). Past and future rainfall in The Horn Of Africa. *Science Advances*, *1*(9), e1500682. https://doi.org/10.1126/sciadv.1500682

Um, M.-J., Kim, Y., Park, D., & Kim, J. (2017). Effects of different reference periods on drought index (SPEI) estimations from 1901 to 2014. *Hydrology and Earth System Sciences*, *21*(10), 4989–5007. https://doi.org/10.5194/hess-21-4989-2017

Vicente-Serrano, S. M., Beguería, S., & López-Moreno, J. I. (2010). A multiscalar drought index sensitive to global warming: The standardized precipitation evapotranspiration index. *Journal of Climate*, *23*(7), 1696–1718. https://doi.org/10.1175/2009JCLI2909.1

Wan, Z., Hook, S., & Hulley, G. (2015). MOD11A2 MODIS/Terra land surface temperature/emissivity 8-day L3 global 1 km SIN grid V006 [Dataset]. *NASA EOSDIS Land Processes DAAC*. https://doi.org/10.5067/MODIS/MOD11A2.006

Wang, M., Menzel, L., Jiang, S., Ren, L., Xu, C.-Y., & Cui, H. (2023). Evaluation of flash drought under the impact of heat wave events in Southwestern Germany. *Science of the Total Environment*, *904*, 166815. https://doi.org/10.1016/j.scitotenv.2023.166815

Warsame, A. A., Sheik-Ali, I. A., Ali, A. O., & Sarkodie, S. A. (2021). Climate change and crop production nexus in Somalia: An empirical evidence from ARDL technique. *Environmental Science and Pollution Research*, *28*(16), 19838–19850. https://doi.org/10.1007/s11356-020-11739-3

Wu, J., Yao, H., Chen, X., Wang, G., Bai, X., & Zhang, D. (2022). A framework for assessing compound drought events from a drought propagation perspective. *Journal of Hydrology*, *604*, 127228. https://doi.org/10.1016/j.jhydrol.2021.127228

Wu, W., Li, Y., Luo, X., Zhang, Y., Ji, X., & Li, X. (2019). Performance evaluation of the CHIRPS precipitation dataset and its utility in drought monitoring over Yunnan Province, China. *Geomatics, Natural Hazards and Risk*, *10*(1), 2145–2162. https://doi.org/10.1080/19475705.2019.1683082

Wu, X., & Jin, S. G. (2014). GNSS-reflectometry: Forest canopies polarization scattering properties and modeling. *Advances in Space Research*, *54*(5), 863−870. https://doi.org/10.1016/j.asr.2014.02.007

Xiang, K., Li, Y., Horton, R., & Feng, H. (2020). Similarity and difference of potential evapotranspiration and reference crop evapotranspiration – A review. *Agricultural Water Management*, *232*, 106043. https://doi.org/10.1016/j.agwat.2020.106043

Xiao, X., Ming, W., Luo, X., Yang, L., Li, M., Yang, P., et al. (2024). Leveraging multisource data for accurate agricultural drought monitoring: A hybrid deep learning model. *Agricultural Water Management*, *293*, 108692. https://doi.org/10.1016/j.agwat.2024.108692

Xu, Z., Li, J., Cheng, S., Rui, X., Zhao, Y., He, H., et al. (2025). Deep learning for wildfire risk prediction: Integrating remote sensing and environmental data. *ISPRS Journal of Photogrammetry and Remote Sensing*, *227*, 632–677. https://doi.org/10.1016/j.isprsjprs.2025.06.002

Xue, Z., Yang, G., Yu, X., Yu, A., Guo, Y., Liu, B., & Zhou, J. (2025). Multimodal self-supervised learning for remote sensing data land cover classification. *Pattern Recognition*, *157*, 110959. https://doi.org/10.1016/j.patcog.2024.110959

Yu, X., Guo, X., & Wu, Z. (2014). Land surface temperature retrieval from Landsat 8 TIRS—Comparison between radiative transfer equation-based method, split window algorithm and single channel method. *Remote Sensing*, *6*(10), 9829–9852. https://doi.org/10.3390/rs6109829

Zhang, C., Zhang, C., Song, J., Yi, J. S. K., Zhang, K., & Kweon, I. S. (2022). A survey on masked autoencoder for self-supervised learning in vision and beyond (arXiv:2208.00173). *arXiv*. https://doi.org/10.48550/arXiv.2208.00173

Zhen, Z., Chen, S., Yin, T., & Gastellu-Etchegorry, J.-P. (2023). Globally quantitative analysis of the impact of atmosphere and spectral response function on 2-band enhanced vegetation index (EVI2) over Sentinel-2 and Landsat-8. *ISPRS Journal of Photogrammetry and Remote Sensing*, *205*, 206–226. https://doi.org/10.1016/j.isprsjprs.2023.09.024

Zhou, Y., Kong, R., Xu, Z., Xu, L., & Cheng, S. (2025). Comparative and interpretative analysis of CNN and transformer models in predicting wildfire spread using remote sensing data. *Journal of Geophysical Research: Machine Learning and Computation*, *2*(2), e2024JH000409. https://doi.org/10.1029/2024JH000409

Zomer, R. J., Xu, J., & Trabucco, A. (2022). Version 3 of the global aridity index and potential evapotranspiration database. *Scientific Data*, *9*(1), 409. https://doi.org/10.1038/s41597-022-01493-1